Electrical High Rate Test

Stephan Wiederkehr
Department of Physics, ETH Zürich

July 29, 2014

Contents

1 Introduction

1.1 LHC and CMS

The Large Hadron Collider (LHC) is the latest and most powerful accelerator added to the European Organization for Nuclear Research (CERN - *Conseil Europen pour la Recherche Nuclaire*). It consists of a 27 km long ring in which 2 beam pipes carry the particles. The particles are forced into a circular path by a magnetic field provided by superconducting electromagnets. There are several accelerating structures along the ring to boost the particle energy. The beams travel opposite to each other and cross in specific areas where detectors are stationed to observe the collision of particles.

One of the four experiments located at the LHC, the compact muon solenoid (CMS) has been designed to search for the Higgs boson and for signs of Supersymmetry alongside the ATLAS experiment. To meet all the requirements of such a task, the CMS detector consists of the following elements, listing from centre:

- a tracking system, including:
  - pixel detector
  - silicon strip detector
- calorimeters, measuring the particles energy:
  - electromagnetic calorimeter (ECAL)
  - hadronic calorimeter (HCAL)
- solenoid
- muon chamber detectors

The solenoid, which is 7 meters in diameter and 13 meters long, provides the experiment with a magnetic field of 3.8 Tesla.
Since the silicon strip detector cannot cope with the design luminosity close to the beam, the innermost detector is made of silicon pixels which can provide three dimensional information of each charged particle.

1.2 Pixel Detector

The CMS pixel detector is designed to measure precise hit information, withstand radiation damage for multiple years of operation and using as little material as possible to minimise multiple scattering of the particles. The barrel part, consisting of three layers and two forward discs are arranged such as to enclose the bunch crossings as good as possible. The described layout of the detector is shown in figure 1. During the winter break in 2016/2017, the pixel detector will be replaced with an 4-layer barrel, 3-disk endcap system. The fourth layer, added at a radius of 16 cm, will increase the tracking precision and also serve as backup in case the first layer of the strip detector degrades faster than expected. The layers are positioned at the radii 30 mm, 68 mm, 109 mm and 160 mm, while the length of the barrel extends to 548.8 mm. The support tube, carrying the pixel modules will also be redesigned to avoid a large increase in material due to the added layer and endcap discs. The detector is built in a modular concept. A module consists normally of 16 readout chips (ROCs). A single ROC has 80 x 52 pixel channels, each of the dimension of 100 μm x 150 μm, yielding a total of 78.8 million channels for the whole barrel part of the detector. To ease the installation of the current detector around the beam pipe, it is built in two halves motivating the construction of half modules.

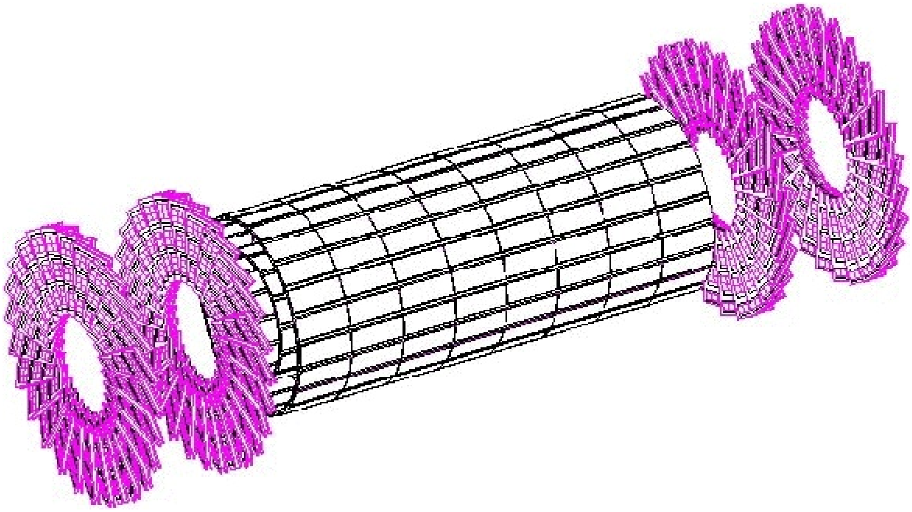

Figure 1: Layout of the pixel detector before the upgrade. The three barrel layers drawn in black and the four forward discs in purple. [2]

1.3 Luminosity

The LHC was designed to operate at a luminosity of $1 \cdot 10^{34} \frac{1}{cm^2 \cdot s}$ while the particle bunches where set to collide every 25 ns. However, when it started in 2009, the spacing between bunch crossings was 50 ns long. Increasing the centre of mass energy led to a peak luminosity of about $7 \cdot 10^{33}\ \frac{1}{cm^2 \cdot s}$ in 2012. If the LHC can keep its level of performance, the luminosity will be further increased along with the centre of mass energy, which is planned to reach 14 TeV. As a next step, the spacing between bunch crossings will be reduced to 25 ns after the first long shutdown (LS1). The development of the luminosity in the past and the predictions for the future can be seen in figure 2. With an increasing luminosity, even going beyond the initial design luminosity, also the pixel detector is confronted with an increasing rate of particle collisions. To cope with the increased requirements, a new chip was designed and is presently under development. It will be installed in the layers 2,3 and 4.

Therefore, in addition to the desire to reproduce hits in a common laboratory similar to those produced in the LHC, also the rate of those hits experiences an increasing importance. Already existing methods to generate high hit rates are the beam test and the X-ray setup. The former can emulate the situation encountered in the LHC very well, but it is a large installation itself, where the latter can be used in a common laboratory, yet it does only induce hits in single pixels instead of inducing hits in clusters, as it happens in the LHC.

The electrical high rate test was developed as a small setup, suitable for laboratories, which can induce clusters of pixel hits. It is the latest method to induce pixel hits at a high rate for testing purposes.[1]

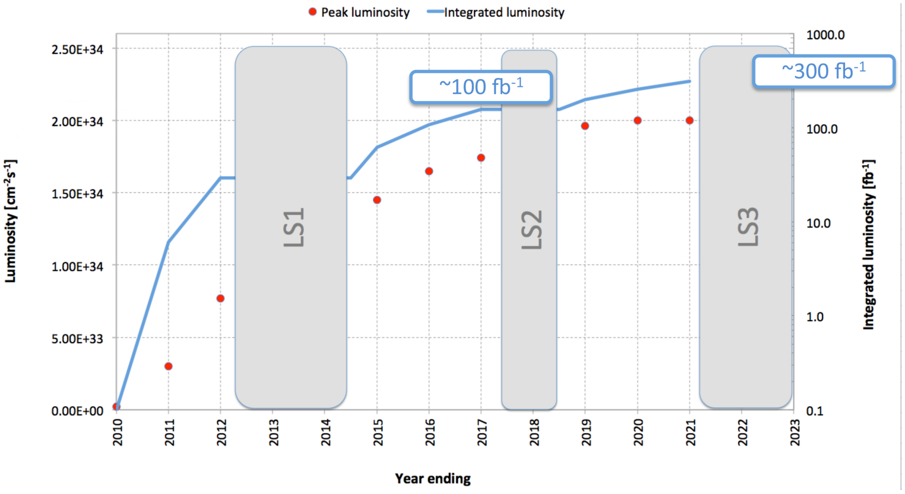

Figure 2: The evolution of the luminosity including the data until and the prediction for the time after LS1. [3]

1.4 Electrical High Rate Test

In the electrical high rate test, hits are induced using electric pulses. These pulses are guided via isolated wires to a Kapton foil which lies on top of the ROC. The Kapton foil acts as a dielectric of a capacitor, such that charge induced on top of it is also induced in the pixel unit cell (PUC) within the ROC. A simple illustration is shown in figure 3. The pulses are generated by a data generator, which allows to define pulse patterns in a tunable pattern length. The used data generator was able to program different patterns into a number of channels, where the pattern length was the same for all channels. Using a pod, each channel could be connected to a bunch of wires, which henceforth will be denoted as cable. Each cable consists of ten wires which were pointing on the previously mentioned Kapton foil. Figure 4 illustrates the explanation above.
All the cables, including the structure to focus the wire on the ROC, are denoted as the excitation harness.

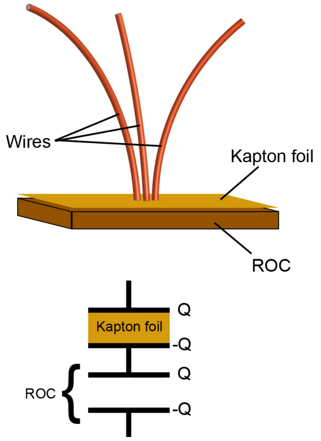

Figure 3: A schematic drawing of the basic principle. Isolated wires pointing on a Kapton foil lying on the ROC. The Kapton foil acts as a dielectric of a capacitor.

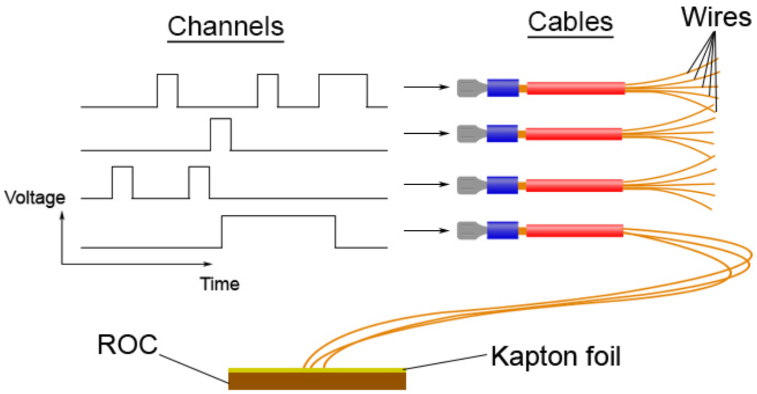

Figure 4: An schematic illustration of the setup, featuring the data generator, the cables, the wires and the ROC. A more detailed description of the setup can be found in section 3.

2 Testing Procedure

The first prototype ready for enhanced measurements of the excitation harness (cf. section 3), which is the pivotal component of the eletrical high rate test, was built at the Paul Scherrer Institute (PSI) before it was brought to the ETH to test it. The goal of this work was to obtain a testing routine to do experiments which require a certain hit rate. Therefore, the first step was to reproduce the basic results of the setup, first and foremost the ability to induce hits in a ROC.

As a second step, mechanisms which influence the rate were identified and investigated. Also the precise procedure and setup for a rate measurement was a priori not clear and was developed. Rate estimates and the deviation from the measurements were analysed, as it is important to provide a desired rate for more advanced measurements.

Finally, the chip efficiency was being tested. The efficiency test analyses the output of the ROC with respect to the input, which is given by the provided rate, and determines the efficiency of the readout process. Such efficiency tests were done before with other methods, e.g. with X-rays. Therefore, the efficiency test was used as a first example making use of a previously defined rate, and it was a good opportunity to compare the results with already established data.

3 Experimental Setup

A picture of the whole setup is shown in figure 5. Also, a schematic is shown in figure 6, where the connections to the particular power supplies are not drawn. In the real setup, a so-called pinboard appears. Its task is to connect cables coming from the pod to the cables of the excitation harness. Hence, the pinboard defines which channel, being output by the pod, is connected to which cable of the excitation harness. A picture taken of the pinboard is shown in figure 7. Another difference between the picture of the real setup and the schematic is the connection between the testboard and the clock input of the data generator. The connection was added after taking the picture and enables the synchronisation of the internal clocks. However, the connection alone does not suffice to synchronise the internal clocks. A description of how the synchronisation can be achieved is given in the section 3.3. Independently of the synchronisation, unless mentioned otherwise, the clock of the data generator was running with 40 MHz, as was the clock of the testboard. Therefore, the data generator could be programmed in units of 25 ns. Unless mentioned otherwise, the minimal pulse length of one clock cycle ($= 25\ ns$) was used to induce hits.

The testboard was, in the end, running with the firmware 2.18. Primarily USB problems, which seemed to be linked to the operating system (Ubuntu), led to installing this version of the firmware.

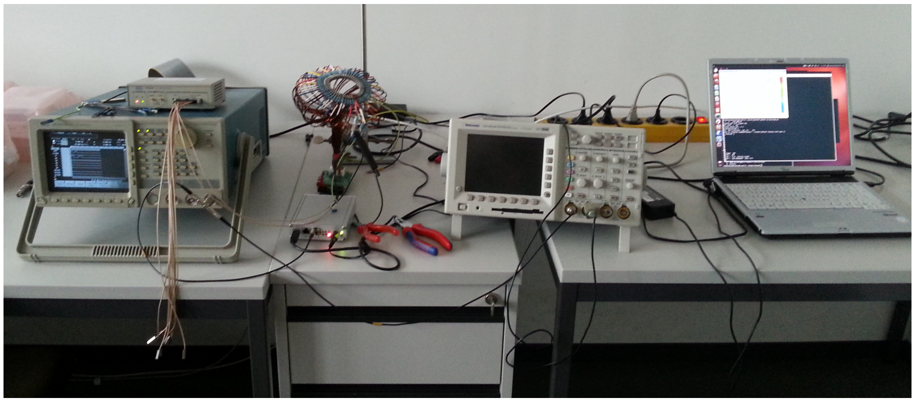

Figure 5: A picture of the whole setup, taken before the first measurements. The connection for the synchronisation of the clock (cf. figure 6) was added later.

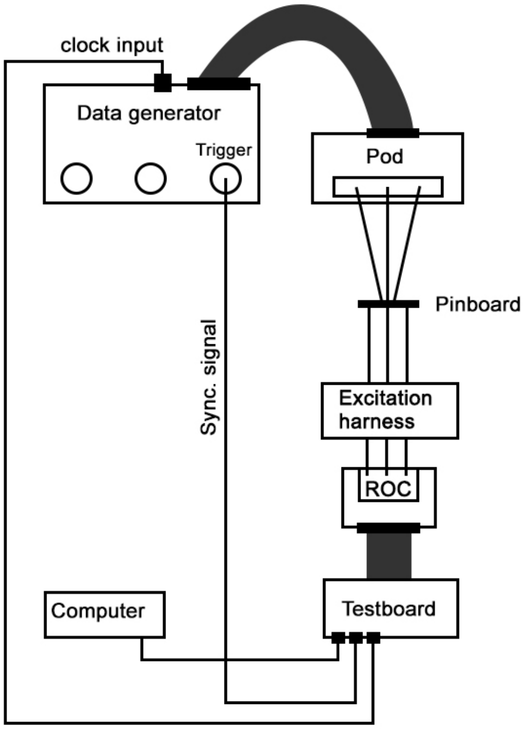

Figure 6: A schematic of the experimental setup.

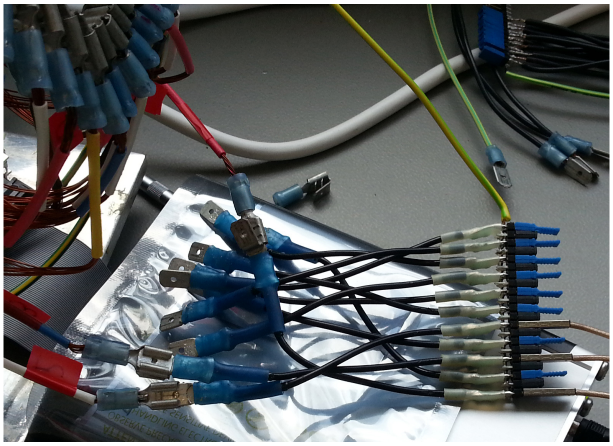

Figure 7: A picture of the pinboard which connects the pod output cables to the cables of the excitation harness. The blue jumpers show possible connections, where the black jumpers suppress a crosstalk between the cables.

3.1 Testboard

The purpose of the testboard is to emulate all commands which can be addressed to a single ROC or even a whole module. The acquired data can be transferred to a computer via a USB connection. A picture of the testboard, taken of its front, is shown in figure 8. There are four LEMO connections on the front of the testboard, where two are fixed connections to put in a clock or a trigger, and thus are labelled CLK and TRG. The other two connections, labelled D1 and D2 can be programmed. Both connections were used in the presented setup. One to put out the clock, the other to put out the synchronisation signal.

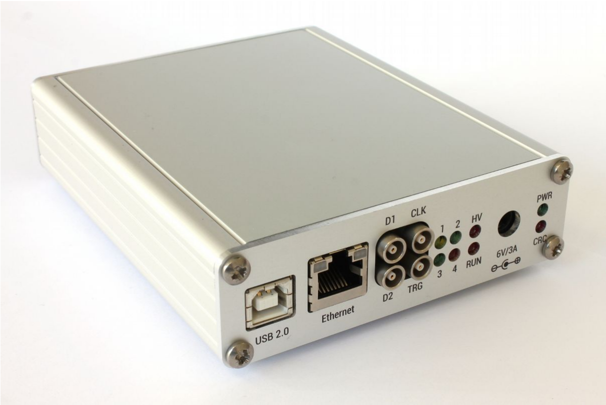

Figure 8: A picture of the front of the testboard.

The single ROC used in this project was wire bonded to a so-called chip board. Furthermore, the chip board was connected to the testboard with an adapter. Figure 9 shows the described setup fully connected. On the adapter, several labelled dot contacts can be identified. With an oscilloscope they can be used to measure the signals corresponding to the labels.

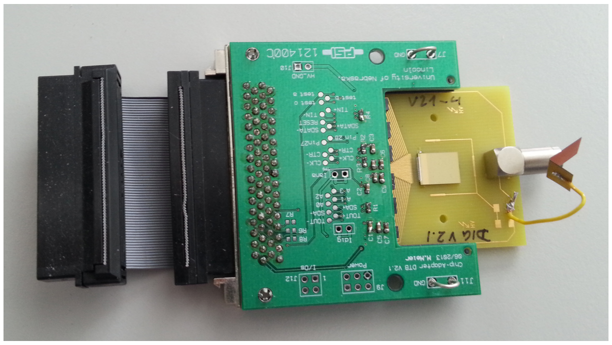

Figure 9: A picture of a single ROC on a chip board. An adapter is connecting the chip board to the testboard. The small installation on the right hand side of the chip board is a basic version of the excitation harness and was not installed for the project presented here.

3.2 Excitation Harness

The excitation harness is the central part of the setup guiding the electric pulses to the ROC and inducing signals in it. Following the previous description, it consists of wires, grouped in cables, which are gathered in a block (of plastic) to focus the wires on the ROC. The Kapton foil is fixed to the bottom of the block. Figure 10 shows a picture of the excitation harness already attached to a ROC. When attaching the excitation harness to a ROC, the block is screwed on the chip board. The chip board is a small printed circuit board (PCB) to which the ROC is wire-bonded. The two drilled holes in the chip board define the position of the block with respect to the ROC. A few splitters of the ROC waver were placed at the sides of the ROC, before screwing the block on top of it, to protect the ROC from pressure. The actual effect of those splitters was not investigated and is not known. As one can see in figure 10, the cables are all connected to each other. This is to connect all of the cables to ground, which is done by the black cable shown in the figure.

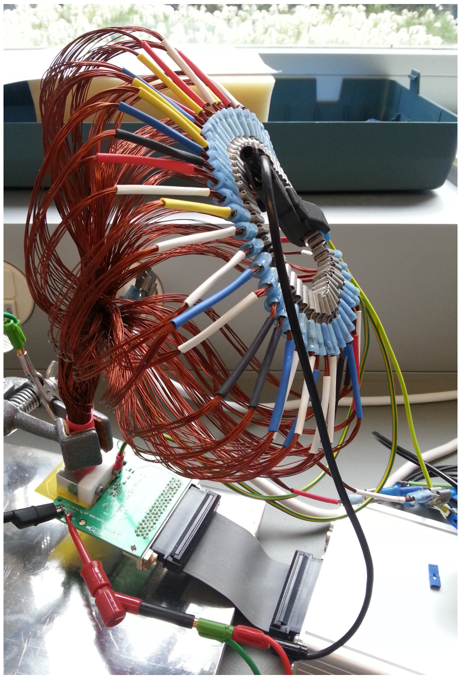

Figure 10: A picture of the excitation harness attached to a ROC. The black cable is the connection to ground.

3.3 DG2020A Data Generator

In this section a more detailed description the the data generator will be given along with a few examples of how to use it. The goal is to help using the presented setup, not to substitute the manual. It is highly recommended to read the latter. The data generator in question was the model DG2020A from Tektronix (Sony), where the pod model was P3410. The figures 11 and 12 show schematics of the front and rear panel of the data generator, respectively. The figure 13 shows a picture of its display while in the EDIT menu.

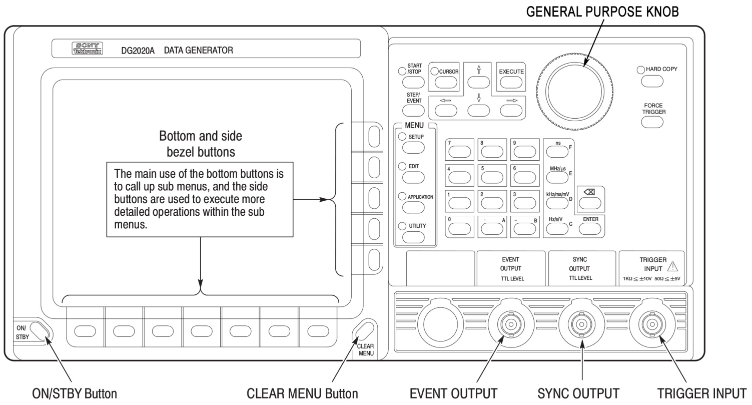

Figure 11: The front panel of the data generator DG2020A. [4]

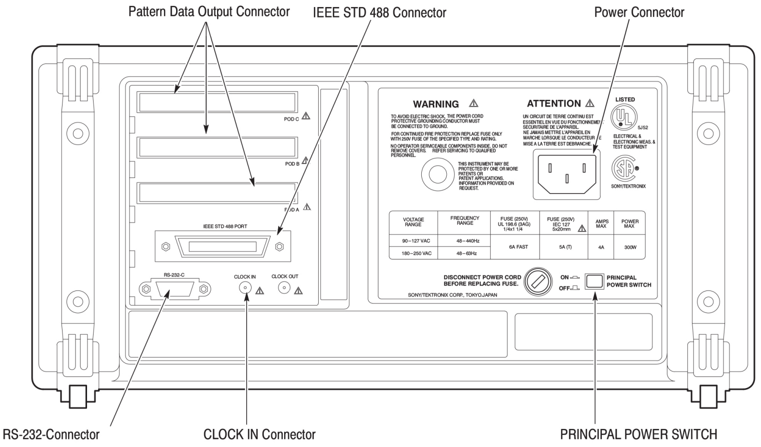

Figure 12: The rear panel of the data generator DG2020A. [4]

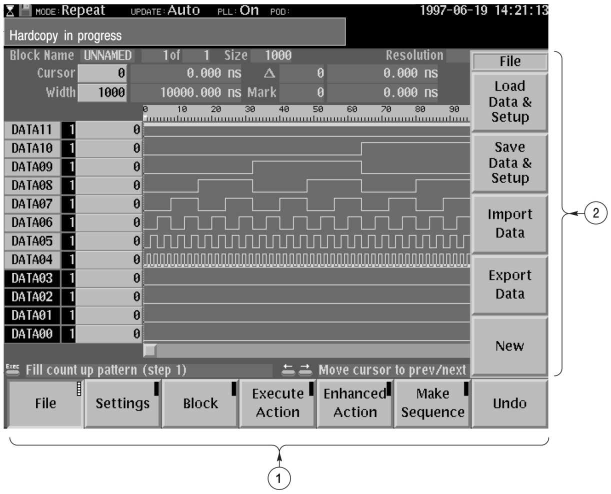

MODE: Repeat UPDATE: Auto PLL: On POD: 1997-06-19 14:21:13

Hardcopy in progress

Block Name UNNAMED 1of 1 Size 1000 Resolution

Cursor 0 0.000 ns △ 0 0.000 ns

Width 1000 10000.000 ns Mark 0 0.000 ns

DATA11 1 0
DATA10 1 0
DATA09 1 0
DATA08 1 0
DATA07 1 0
DATA06 1 0
DATA05 1 0
DATA04 1 0
DATA03 1 0
DATA02 1 0
DATA01 1 0
DATA00 1 0

Exec Fill count up pattern (step 1) Move cursor to prev/next

Figure 13: The display of the data generator DG2020A showing the typical content of the EDIT menu.
(1) and (2) are controlled via the bottom and side bezel buttons, respectively. [4]

Connecting the DG2020A:
To use the data generator only the power connector needs to be connected while the principal power switch must be switched on (cf. figure 12). To output channels, a pod needs to be connected to one of the three pattern data output connectors. The clock synchronisation can be achieved by connecting the testboard to the *clock in* connection. Note that the testboard supports LEMO connections, while the *clock in* supports SMB connections. Once a pod is connected, the channels of the data generator must be assigned to the pod outputs. The assignment is explained below. To navigate through the menus described in the following, use the bottom and side bezel buttons (cf. figure 11).

Setting the internal clock:
Enter the SETUP menu and open the OSCILLATOR menu. First the source can be chosen. To synchronise the clock with the testboard clock, choose EXT. To enable the generation of an internal clock, select INT. If an internal clock is used the PLL should be turned ON. If an external clock is used the PLL must be turned OFF. Using an internal clock, its frequency can be chosen pressing INT FREQUENCY. If an external clock is used, the EXT FREQUENCY influences the displayed frequency, e.g. in the EDIT menu, and should therefore be chosen as close as possibly to the actual external frequency.

Editing the channels:
To edit the channels enter the EDIT menu. Subsequent, a display will appear similar to figure 13. The leftmost entry in each row displays the name of the channel. The pattern length can be edited pressing SETTINGS → SET MEMORY SIZE. The memory size is then entered in units corresponding to the pattern unit length, which is 25 ns if the internal clock has been set to match the clock of the testboard. To edit a pattern, select EXECUTE ACTION → SET DATA TO HIGH or SET DATA TO LOW. Select the channel using the arrow buttons. Then use the general purpose knob or the arrow buttons to select the bit and press the EXECUTE button to edit the bit. To edit multiple bits at once in the same channel, press the CURSOR button, change the cursor size with the general purpose knob and press the CURSOR button again.

Editing the run mode:
To choose the run mode, select the SETUP menu and press RUN MODE. Now, a variety of run modes can be selected, where the most important ones

are the REPEAT and the SINGLE mode. To send the patterns repeatedly, select REPEAT. If the trigger (which the testboard sends to the ROC) shall be synchronised with the pattern, select SINGLE. The SINGLE mode will send the pattern once (!) each time the data generator receives a trigger (corresponding to the synchronisation signal output by the testboard) in the trigger input (cf. figure 11).

Assigning channels to the pod:
Press the SETUP button and select the POD ASSIGN menu. This opens a new window in which the general purpose knob can be used to select the internal channels (e.g. DATA01). The arrow buttons are used to select the output channel of the pod (e.g. A-01).

Press the START/STOP button to start or stop the output of the pulse patterns.

3.4 Rate Estimate and Measurement

It is very important, for the understanding but also to program the data generator accordingly, to be able to estimate the hit rate. In principle, the rate corresponds to $\frac{\#hits}{time}$. Since for all rate measurements the data generator sent the programmed pulse pattern repeatedly and without a delay between two patterns, the relevant time is the pattern length. Within the pattern length, the amount of hits is given by the amount of hits generated by each pulse multiplied by the amount of pulses. This is summarised in equation 1, where N_p is the amount of pulses, N_h is the number of hits per pulse, M is the pattern length given in μs and A_{ROC} is the area of the ROC. With a desired rate given, the formula can be applied to estimate the pattern length and the amount of pulses to place in it.

$$rate\,[\frac{MHz}{cm^2}] = \frac{N_p \cdot N_h}{M} \cdot \frac{1}{A_{ROC}} \tag{1}$$

To measure the rate, a sequence consisting of a CAL (calibrate), a TRG (trigger), a TOK (token) and a delay was sent to the ROC.
The CAL signal injects charge in a pixel to emulate a hit. Unless the pixel is *armed*, though, the charge is not being switched through, such that it does not influence the pixel. The TRG signal indicates the data to be readout, before the TOK signal starts the readout process. The data readout with one trigger is sometimes also called an *event*. In general, an event may or may not contain hits. In the following, events containing hits are labelled

non-zero events.
The delay consisted of a fixed part and a random contribution. The fix delay was set to 10 μs to provide enough time for the chip to read the data out. The random part varied between 0 and 50 μs.

The sequence can be sent in two ways, either via the Pg_Single command or via the Pg_Loop command.
The Pg_Loop command sends a defined sequence and a defined delay repeatedly. The user can define the start, the time during the command shall run and the stop. The amount of sent triggers can be calculated using the time of one loop (sequence + delay) and the duration of the command. Since the calculation may differ from the actual amount of triggers sent, the Pg_Single command was used.
The Pg_Single command sends the afore defined sequence one. Hence, to send e.g. 1000 triggers, the Pg_Single command must be executed 1000 times.

It was found, that sending those single shots led to an additional, not constant delay.
Therefore, the total delay amounted to about 275 μs on average, corresponding to a trigger rate of roughly 3.6 kHz. The triggers were sent to the testboard using a single command. However, in the test program, the total amount of triggers was split up using a *for loop* as shown in the pseudo code below. In the following, the amount of loops. inside such a *for loop*, will be referred to just as *loops.*

```
$for\ (loops)$
    $send(x\ sequences\ (each\ sent\ as\ Pg\_Single))$
```

The random delay and the loops were applied to randomise the readout. Ideally, the hits would occur randomly. However, since they have to be programmed and therefore are not random, the readout was randomised instead.

The program measuring the rate (cf. the appendix) essentially executed the *for loop* shown above, collected the data and calculated the rate. The data contained the amount of events corresponding to the number of triggers sent.
Each event comprised the amount of hits, including the information about

the their pulse height (not calibrated) and their pixel address.
The rate was calculated by dividing the number of hits and by the total number of triggers (*loops* $\cdot$ *#triggers per loop*) according to equation 2, where N_{hits} is the amount of hits, N_{trg} is the amount of triggers, τ (= 25 ns) is the clock cycle length, A_{ROC} is the area of the ROC and C (= 40) converts the rate from $\frac{40\ MHz}{cm^2}$ into $\frac{MHz}{cm^2}$.

$$rate\ [\frac{MHz}{cm^2}] = \frac{N_{hits}}{N_{trg}} \cdot \frac{1}{\tau} \cdot \frac{C}{A_{ROC}} \tag{2}$$

4 Results

4.1 Early Results/Proof of Concept

The result of an early rate measurement is shown in figure 14. The figure shows a map of the ROC where the amount of hits is plotted as a function of position. Indeed, each wire induces a cluster of roughly 10 pixel hits. However, only eight clusters can be seen, even though ten clusters were expected after connecting one cable.
Unfortunately, the observation of less than ten wires was the generic case. The reasons were found to be one of the following:

- The wires did not point on the ROC.
- The wires were not close enough to the Kapton foil, let alone touching it. This is discussed further in the section 6.
- The wires were broken or badly soldered.

Figure 15 shows a distribution of non-zero events per loop, where an event describes a readout clock cycle. As the readout process is assumed to be random, a Poisson distribution was expected. Furthermore, since the depicted mean corresponds well to the maximum of the distribution, the mean is equivalent to the probability to encounter a non-zero event in a loop. The probability can be read off dividing the mean by the number of triggers per loop, in this case 1000. This probability can be compared to the probability given by the data generator. The latter is simply the amount of pulses divided by the pattern length, assuming a pulse induces hits in only one clock cycle.

As an example:
The measurement shown in figure 15 was done with 1000 triggers per loop,

which corresponds to a probability of 1.724 %.
The measurement was done with only one cable. The pulse pattern was 58 clock cycles long and contained one pulse of one clock cycle. Therefore, the expected probability is equal to $\frac{1}{58} \approx 1.724$ %.

Generally, a good agreement between those probabilities was found. Hence, the clock cycles were, roughly, readout equally often, confirming the assumption of a random readout.

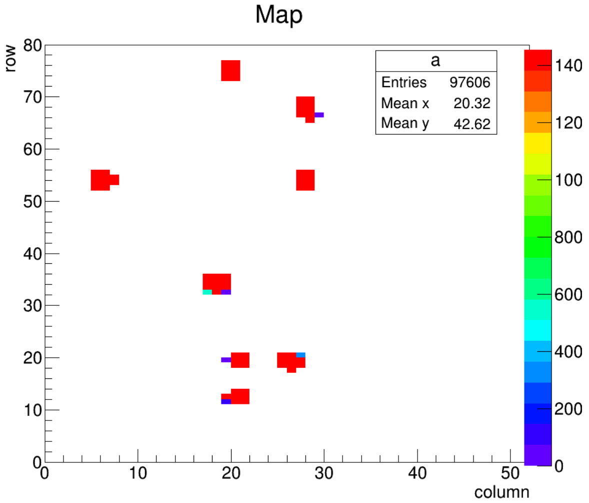

Figure 14: The typical outcome of a rate measurement. Only one cable is connected. The amount of hits is plotted as a function of position.

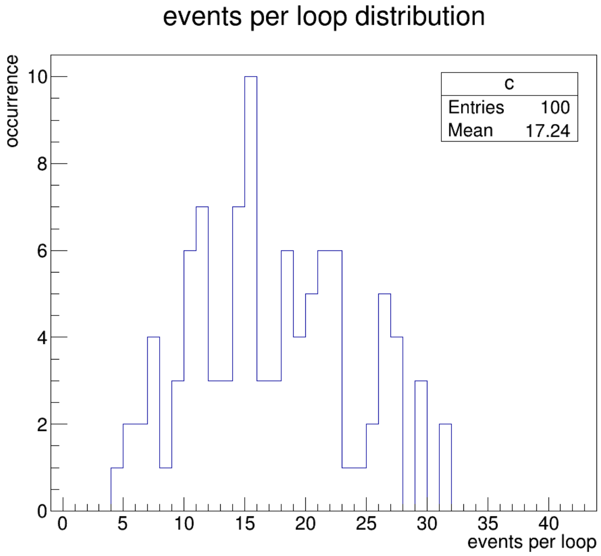

Figure 15: A distribution of non-zero events per loop. 1000 triggers were sent in 100 loop.

4.2 Clock Synchronisation

At this stage, every pulse, of the length of one clock cycle, was assumed to induce hits in only one clock cycle. Calculations as in the example of the previous section are based on this assumption. When the hits per event distributions were plotted, two clear peaks were expected. One at zero, the other at about 80 hits, since:

$$8\ clusters\ \cdot\ 10\ hits\ per\ cluster = 80\ hits$$

However, measurements done with the clocks from the testboard and the data generator running asynchronously, led to the detection of so-called low-hit-events (LHE).
Thereafter, the clocks were always synchronised by putting the clock of the testboard into the data generator (cf. sention 3.3). To put the clock out of the testboard, one of the programmable outputs (labelled D1/D2) had to be programmed accordingly before each test. Examples of how to program this are contained in the appendix.

The figure 16 shows two hits per non-zero event distributions for the asynchronous and the synchronous case. Aside from the synchronisation of the clock, these two distributions were obtained using the same test parameters. In the asynchronous case, there are LHE on the left of the clear peak. Also, the total number of entries was significantly larger. However, the rate stayed, within the measurement error, the same.

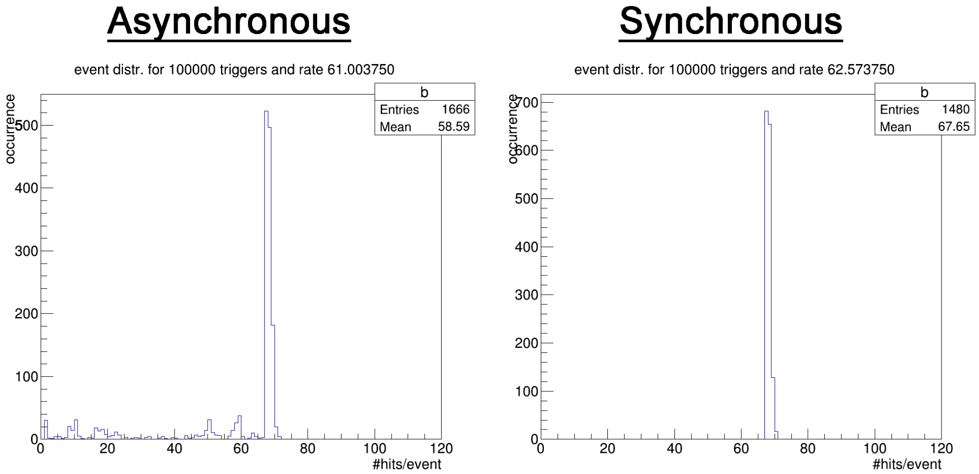

Figure 16: A hits per non-zero event distribution for each, the asynchronised clock and the synchronised clock case.

A closer look at LHE revealed the data shown in the figures 17 and 18, where the former displays a ROC map of only one non-zero event and the latter shows the result of the whole rate measurement containing all hits. As can be seen in the two figures, the LHE are in the same clusters as usual non-zero events. In figure 18 the difference between a LHE and an expected non-zero event can clearly be distinguished by the amount of hits and therefore the colour in which they are plotted. The green pixels correspond to an expected hit belonging to the peak in the distribution on the left of figure 16. The red pixels saw additional hits coming from LHE of the mentioned distribution. It is unclear, why the LHE manifest themselves only in some pixels instead of being equally distributed over all clusters.
The contribution of LHE to the rate was roughly up to 40 %, where the percentage did depend on the cable. To emphasise this, figure 19 shows a measurement for another cable.

The pulse height of LHE did appear to be randomly scattered within the expected pulse height distribution as a change in the comparator threshold did not extinguish the LHE. Neither did the relative contribution to the rate change significantly. It was not investigated whether the pulse height of a particular pixel changes when the pixel is part of an LHE w.r.t. when it is part of an usual hit.

It is being assumed that running the clock asynchronously “splits” some pulses into two clock cycles, where each contains a fraction of the total amount of hits. This would explain the increased number of non-zero events, as well as the occasionally reduced amount of hits within such an event. The LHE were not investigated more intensely and remain not fully understood, though.
The probability of a non-zero event, as discussed in the previous subsection, was significantly influenced by LHEs, and therefore impaired a comparison with estimates. Since such comparisons were exceedingly important at this stage of the experiment, the clocks were synchronised for all following test, unless mentioned otherwise.

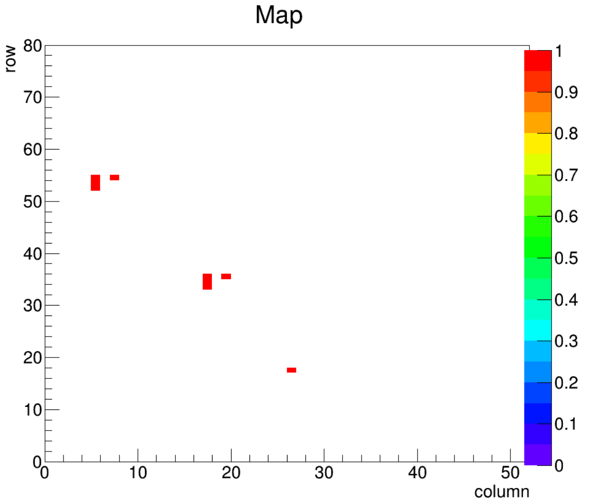

Figure 17: A ROC map displaying a single LHE. The amount of hits is plotted as a function of position

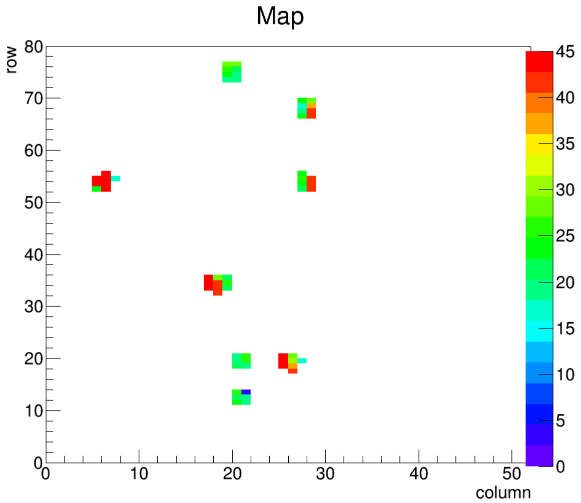

Figure 18: A ROC map, where the amount of hits is plotted as a function of position. The red pixels indicate LHE, while the green pixels indicate an expected hit corresponding to the peak in figure 16.

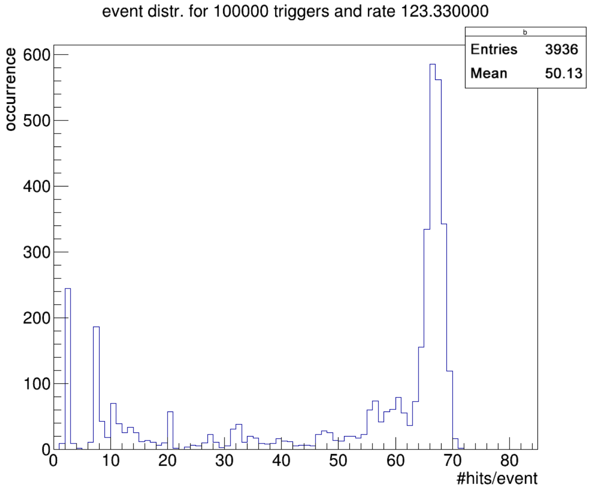

Figure 19: A hits per non-zero event distribution. The difference to the data shown in figure 16 is the amount of pulses used and the connected cable.

4.3 Pulse Height

As whole clusters of hits are induced, it was a priori not clear how the pulse height would be distributed. Beforehand, a pulse height calibration was done to assign an amount of charge to the digital value delivered by the pixel.
Figure 20 shows a ROC map, where the pulse height was plotted as a function of position. From the figure it becomes clear that the pulse height is not uniform over a cluster which leads to the broad pulse height distribution shown in figure 21. As a consequence, the rate can be tuned gradually by varying the comparator threshold. Figure 22 shows a plot, where the rate is plotted as a function of the comparator threshold. Indeed, the increase in the rate is gradual until the threshold is on the level of the noise, which occurs at a $V_{thrComp}$ value of about 135. $V_{thrComp}$ is a digital to analogue converter (DAC) which determines the height of the comparator threshold.

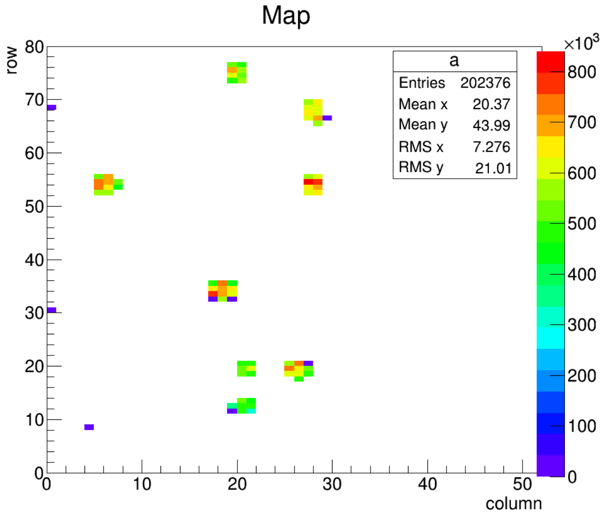

Figure 20: A ROC map. The pulse height is plotted as a function of position.

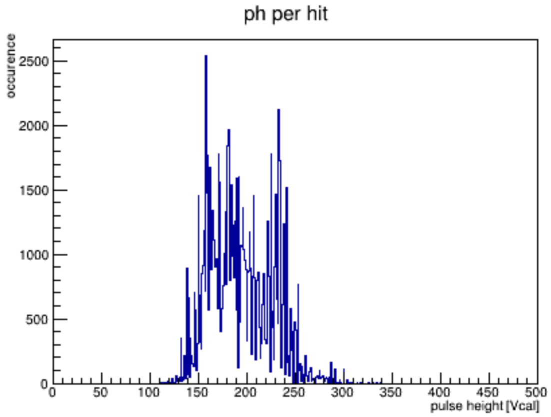

Figure 21: A typical distribution of the pulse height per hit.

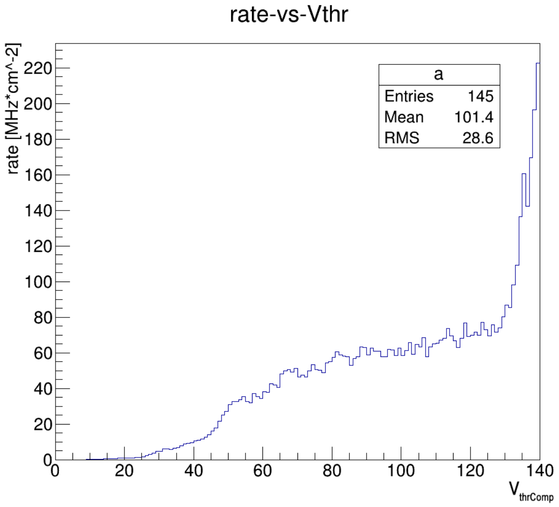

Figure 22: The rate is depicted as a function of the comparator threshold.

4.4 Pulse Length

While the early measurements where done with a haphazardly chosen pulse length, the necessity of a proper investigation of its influence became pressing subsequently.

It was impossible, though, to analyse particular clock cycles with a random trigger. Therefore, the trigger and the pulse had to be synchronised. The synchronisation was achieved by adding a synchronising signal to the sequence, as depicted schematically in figure 26. One of the programmable outputs of the testboard was programmed to put out the synchronisation signal as it was done with the clock (cf. section 4.2). This particular signal output was then connected to the trigger input of the data generator which was programmed as to send the sequence only once after receiving the synchronisation signal from the testboard (cf. the paragraph about the run mode in section 3.3).

Since the synchronisation signal was synchronous w.r.t. to the (testboard) trigger and w.r.t. the pulse of the data generator, the trigger was synchronous w.r.t the pulse.

As illustrated in the schematic, the WBC value determines which clock cycle is read out while the *tct* value determines the distance between the calibrate signal and the trigger signal. In the following measurements the *tct* value, instead of the WBC value, was varied to scan through the region of the pulse. The usage of the *tct* value or the WBC value is equivalent, and the unit of both values is given in clock cycles.

The figures 23, 24 and 25 show the amount of hits plotted as a function of the *tct* value for different pulse lengths. As mentioned before (cf. section 3), the unit length of the pulse length is given in clock cycles as well.

In figure 23, it is clear to see, that there are only hits in one clock cycle when using the smallest possible pulse length. On the other hand, figure 25 indicates clearly, that the rising edge as well as the falling edge cause hits. Keeping this in mind, the contribution of the rising edge as well as the falling edge can also be identified in figure 24. However, there are also hits in between the two edges. The contribution of hits in between the edges was found to be largest at pulse lengths of about 5-7 clock cycles. At a pulse length of about 25 clock cycles, this contribution is very small, yet, further increasing the pulse length does not necessarily extinguish this contribution. It can be avoided, though, by increasing the comparator threshold. In the same way the whole contribution from the rising edge or the total contribution from both edges can be erased. All performed pulse length

measurements are shown in the appendix.
In the schematic in figure 26 also the pulse, as it is assumed to behave inside the ROC, is drawn along with the comparator threshold voltage. The chip is designed such that it reacts only on falling edges. Therefore, whenever a falling edge crosses the level of $V_{thrComp}$, a hit is induced in a pixel. Thus, in theory, only the falling edge of the pulse was expected to induce hits. The contribution of the rising edge, as well as the contributions in between the edges are attributed to the post flank oscillations. It is, however, not understood how these oscillations cause what is depicted in figure 24 and 25.
For instance in figure 25, and considering the schematic, it is unclear how in the contribution of the rising edge (pulse) even the second falling edge (post flank osc.) seems to induce hits, while in the contribution of the falling edge (pulse) only the first falling edge (post flank osc.) induces hits.

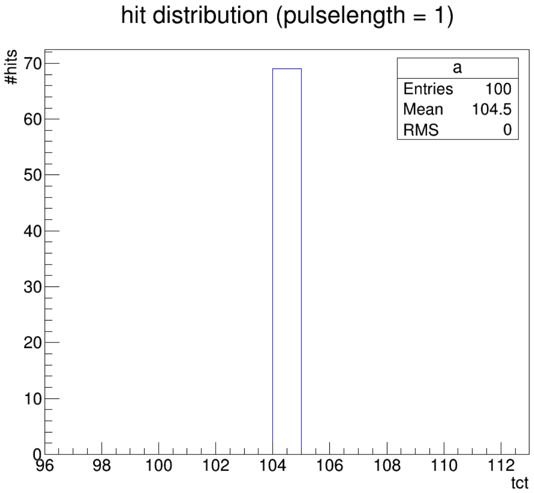

Figure 23: The amount of hits as a function of *tct*. The unit length of a pulse is 25 ns.

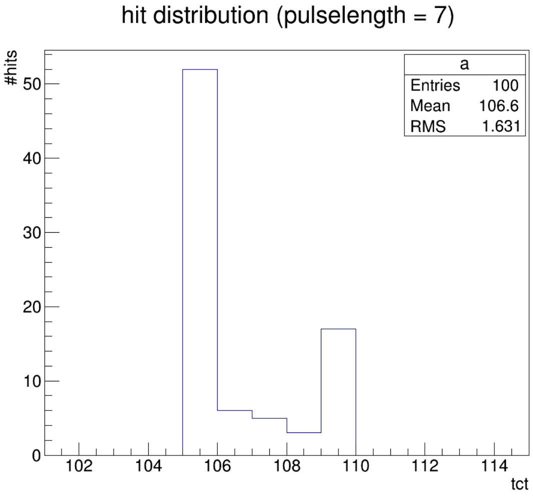

Figure 24: The amount of hits as a function of *tct*. The unit length of a pulse is 25 ns.

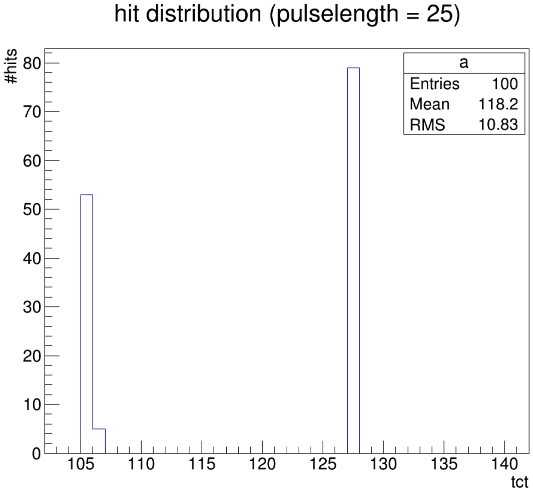

Figure 25: The amount of hits as a function of *tct*. The unit length of a pulse is 25 ns.

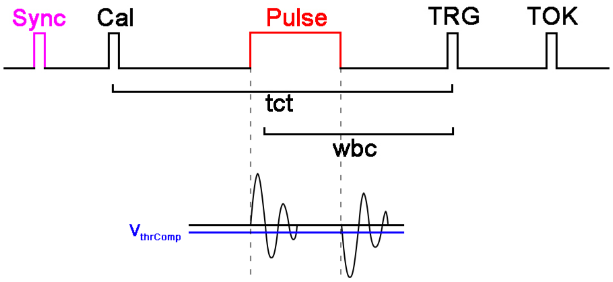

Figure 26: A schematic of the signal synchronisation. Additionally, the post flank oscillations are drawn.

4.5 Rate Measurements

As the hit rate is generated by the pulse pattern, which was sent repeatedly during rate measurements, the exact rate is given by reading out all clock cycles of the pulse pattern once and averaging the hits contained in them. For a random readout this means that every clock cycle of the pulse pattern should be read out equally often. Hence, the amount of statistics determines the precision of the rate measurement.
It was found, that at least 100,000 triggers have to be sent to achieve a reasonably small error. Moreover, the influence of the loops was found to be significant. Figure 27 shows the distribution of 600 rate measurements, all done with 100 loops and 1000 triggers each. Figure 28 shows a similar distribution, but the measurements were done with only one loop and 100,000 triggers in it. The total amount of triggers in the measurements of both distributions is therefore the same. However, the root mean square (RMS) shown in the inset box in each distribution indicates that the loops do contribute significantly to the randomness of the readout. For comparison, table 1 shows the mean and the RMS for different settings.

Using measurements, such as the hits per non-zero event distribution, to get more precise information than merely vague estimates, the formula in equation 1 yielded values very close to the measured rate. The formula proved to be the most accurate way to program the data generator to provide a certain hit rate. Due to the finite width of the mentioned hits per non-zero event distribution and the error in the measured rate, a fine tuning of the data generator was necessary in most cases.

It should be noted that the rate can only be measured correctly with a pixel efficiency close to 100 %. Increasing the rate will lead to a strong decrease in the pixel efficiency which will finally reach 0 % such that the measurable rate has an upper limit. This limit could be overcome by inducing hits in double columns which were previously not hit by any clusters. This means, that the upper limit depends on the choice of cables.
Hence, this limitation is attributed to an overflow in the double column data buffer. Since each cable induces up to ten clusters, which might all lie in the same double column, this limit can occur at relatively low rates, e.g. at about 100 $\frac{MHz}{cm^2}$. Therefore, this limitation should always be considered when choosing cables for a rate measurement.

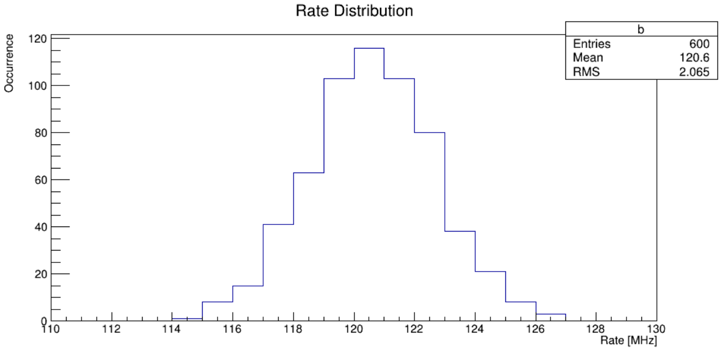

Figure 27: A distribution of 600 rate measurements, all done with 100 loops and 1000 triggers each.

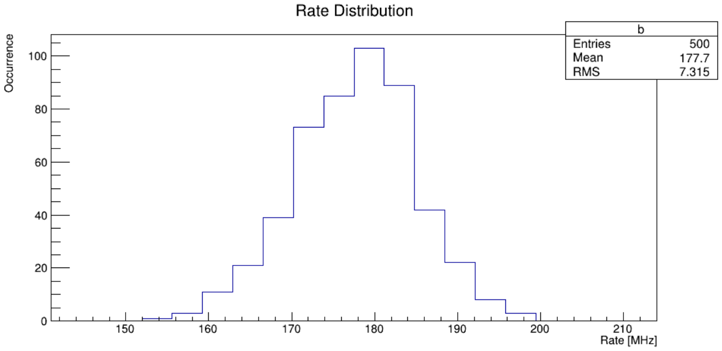

Figure 28: A distribution of 500 rate measurements, all done with 1 loop and 100,000 triggers each.

Table 1: The mean and RMS of rate distributions for different settings.

Measurements	loops	triggers per loop	mean rate $[\frac{MHz}{cm^2}]$	RMS $[\frac{MHz}{cm^2}]$
100	10	10	124.8	83.56
100	100	10	141.48	33.13
100	10	100	128.91	45.83
100	100	100	115.74	9.14
100	100	1000	136.47	4.07

4.6 Desynchronisation

There were reports of an issue when reading out data. Specifically, it seemed that data belonging to one trigger were readout with the next or the previous one. This shift, which is called desynchronisation, could also be investigated with the current setup. To do so, a new sequence (cf. section 3.4) was defined consisting of the following signals.

$$\mathbf{CAL} + \mathbf{TRG} + \mathbf{TOK} + delay + \mathbf{TRG} + \mathbf{TOK} + delay$$

The delay was 510 clock cycles long, the time between CAL and TRG (*tct*) was 106 clock cycles long and the time between TRG and TOK (ttk) was 32 clock cycles long.
A particular pixel was armed, such that the voltage defined by V_{Cal} was switched through and read out by the first trigger, only. At the same time the data generator was providing pulses at an afore determined rate. The address of the armed pixel was chosen not to lie within a cluster, such that the test could search for a particular pixel address to identify the V_{Cal}.
As the readout was random, both triggers may or may not contain hits due to the electric pulses. The CAL signal was, however, a fix part of the sequence such that the V_{Cal} was expected in *every* even trigger, as the counting started at zero.
The first test did break when encountering the first error and produced four ROC maps in total, each plotting the amount of hits as a function of position. An error was produced when either the V_{Cal} was found in an odd trigger, or no V_{Cal} was found in an even trigger.
The first map contains all hits gathered during the test. The map labelled "error" contains the data belonging to the trigger which produced the first error, while the maps labelled "previous" and "after first error" contain the data belonging to the trigger preceding or following the error, respectively. Figure 29 shows the outcome of two measurements. In the measurement on the left the V_{Cal} simply vanished, while in the measurement on the right the V_{Cal} was shifted to the next (odd) trigger.

The error was typically found after $300,000 \pm 50,000$ triggers and did not depend on the rate, as it also occurred with the data generator turned off. As a first step, the data flow on the testboard was changed. This was done by increasing the parameter *buffsize* from its default value (2097152) to 5,000,000 and additionally increasing the parameter *blocksize* successively, starting at its default value 8192.
As a result, increasing those parameters did also increase the trigger num-

ber at which the first error occurred. At the value *blocksize* $= 1,000,000$ no error was found during ten measurements, each sending 2,000,000 triggers.

The figures 30 and 31 show essentially the same test, though it was modified not to stop at the first error, but to plot all the events in a certain range around it. The hits caused by the electric pulses are clearly visible as those events contain more than the one hit due to the V_{Cal}. The entries plotted in green correspond to events which passed the error test, while the entries plotted in read produced errors according to the definition above. To see errors at all, the *blocksize* was set to its default value again.
Figure 31 is particularly interesting, because the V_{Cal} returned to the even events after a period in which it was found in the odd events. It is not clear whether the V_{Cal} shifted twice in the same direction, or if it shifted back and, therefore, restored the original synchronisation.

In summary, the desynchronisation was not found to depend on the hit rate. Only the *blocksize* and *buffsize* values were found to influence the appearance of the effect. The desynchronisation was not further investigated, because it did not appear with the blocksize and buffsize values mentioned above.

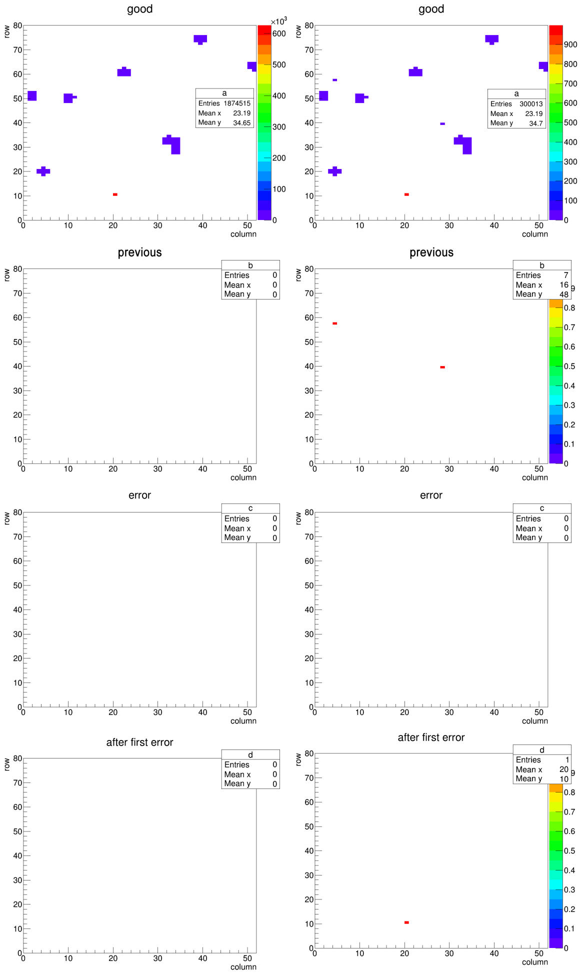

Figure 29: Two desynchronisation measurements. The amount of hits is plotted as a function of position.
Left: The V_{Cal} expected in an even trigger vanished. The precedent and following trigger contain no V_{Cal}, as expected.
Right: The V_{Cal} expected in an even trigger was shifted into the following, odd trigger.

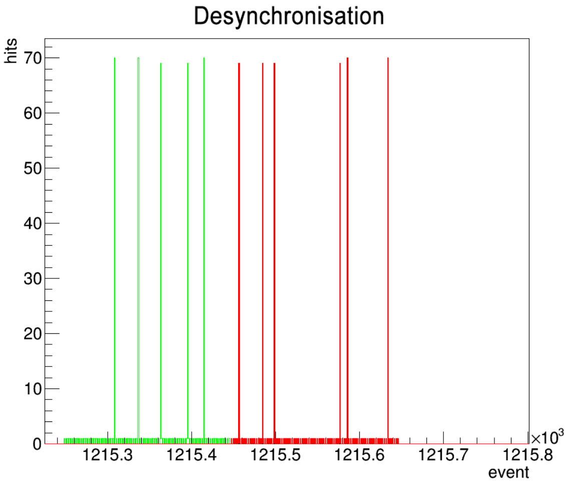

Figure 30: A desynchronisation measurement. The amount of hits is plotted as a function of the event.

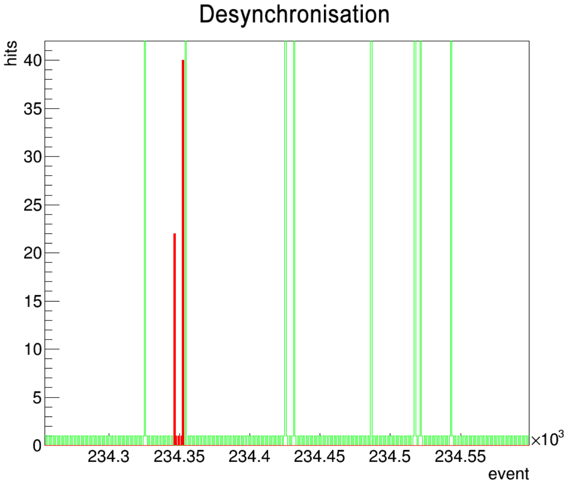

Figure 31: A desynchronisation measurement. The amount of hits is plotted as a function of the event.

4.7 Chip Efficiency

After the hit rate was well understood and a procedure was found to produce a desired rate, the next step was to use the acquired knowledge to perform a more advanced test. The more advanced test was in fact an early chip efficiency test, for which the setup was built.

The efficiency of a pixel was tested by switching through a V_{Cal} and reading it out again, while the chip had to deal with the hits induced by the data generator. Therefore, the efficiency of a pixel corresponds to the readout V_{Cal}s divided by the total amount of V_{Cal}s sent. The latter is equivalent to the total number of triggers sent, since the sequence sent to the chip was the same as for a rate measurement (cf. 3.4).
Therefore, the efficiency corresponds to the following formula, where N_{Cal} is the number of readout V_{Cal}s and N_{trg} is the number of triggers.

$$pixel\ efficiency = \frac{N_{Cal}}{N_{trg}}$$

All pixels of the ROC could not be armed at once, due to memory limitations, but it was armed row by row. The full procedure of a test was the following:

- A single reset signal was sent.
- A whole row of pixels was armed and another single reset signal was sent.
- The sequences were sent to the ROC. A total of 100,000 triggers were sent in 100 loops and 1000 triggers each.
- The readout V_{Cal}s were plotted in a ROC map as a function of position.
- The whole ROC was unarmed and the procedure started anew. After the last row the test ended.

According to the procedure, the outcome of such a test was a ROC map where the pixel efficiency was plotted as a function of position. Figure 32 shows a so-called efficiency map at a hit rate of 300 $\frac{MHz}{cm^2}$. As one can see by the clusters of lesser efficiency, these tests were performed using five cables to distribute the clusters over the whole ROC. The analysis is shown in figure 33. One can clearly see a peak at 100 %. In addition, on the left a separate region can be distinguished. The pixels in this region belong to

the particularly affected double column in figure 32. The mean efficiency of such a test was then extracted and plotted against the rate, as shown in figure 34.
The error in the rate was taken from the rate distribution in figure 27. The error in the efficiency was taken from the distribution in figure 35, where the distribution of 30 efficiency test is shown. The efficiency tests for this distribution were, however, done only over the rows 40 - 60 to decrease measurement duration.

In figure 34, the efficiency does not change, within the error, as the rate increases from 300 to 350 $\frac{MHz}{cm^2}$. This is attributed to the method used to increase the rate to 350 $\frac{MHz}{cm^2}$.
In section 4.5, an upper limit to the measurable rate is mentioned. This limit was reached soon after 300 $\frac{MHz}{cm^2}$. To increase the rate anyway, two of the five cables were chosen which had a negligible overlap in terms of affected double columns. This means that the clusters of those two cables did lie in different double columns such as not to increase the data in the double column data buffers. To increase the rate, an additional pulse was sent to one of those cables at the same time when a pulse was sent through the other cable. This situation is schematically shown in the schematic on the right.

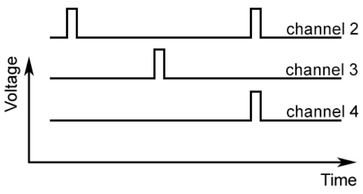

This method allowed the measurement of a higher rate. On the other hand, a further drop in the efficiency of the strongly affected double column, shown in figure 32, was clearly avoided as the additional hits were all in other double columns.

Figure 36 shows the efficiency and the local rate as a function of the double column in the left column, and the efficiency as a function of the local rate in the right column. The plots contain the data for the rates 253 $\frac{MHz}{cm^2}$, 300 $\frac{MHz}{cm^2}$ and 353 $\frac{MHz}{cm^2}$, as these were the least expected results. The remaining data can be found in the appendix.
The local rate was calculated as in equation 3, were N_{hits} is the number of hits, N_{trg} is the number of triggers, τ is the clock cycle length, A_{DC} is the area of the double column and C converts the rate to MHz.

$$local\ rate\ [\frac{MHz}{cm^2}] = \frac{N_{hits}}{N_{trg}} \cdot \frac{C}{\tau \cdot A_{DC}} \tag{3}$$

The efficiency was expected to decline steadily as a function of the local rate. Yet, the difference in efficiency between the double columns at a relatively low local rate is too large to see any tendency. The only clearly visible decline was observed if the local rate exceeds 16 $\frac{MHz}{cm^2}$ per double column at a total rate of 300 $\frac{MHz}{cm^2}$. There, the efficiency dropped below 40 %. Including the data for 353 $\frac{MHz}{cm^2}$, the reason for this jump becomes unclear.
Contrariwise, it is not understood why, at 353 $\frac{MHz}{cm^2}$, there are two double columns which have an efficiency over 90 % at a local rate of over 16 $\frac{MHz}{cm^2}$. Especially, since the the local rate did not decrease, compared to the measurement done at a total rate of 353 $\frac{MHz}{cm^2}$.

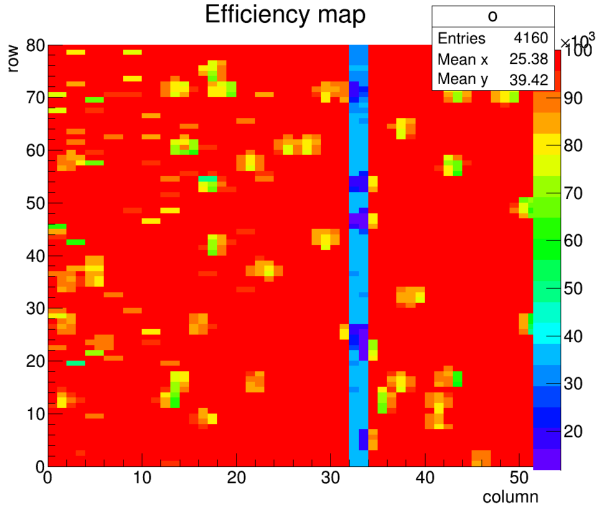

Figure 32: An efficiency map at 300 $\frac{MHz}{cm^2}$. The amount of readout V_{Cal}s is plotted as a function of position.

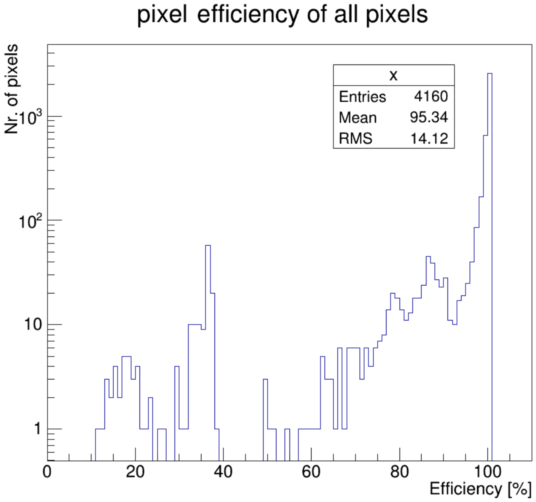

Figure 33: The analysis of the pixel efficiency map at 300 $\frac{MHz}{cm^2}$. The number of pixels as a function of their efficiency.

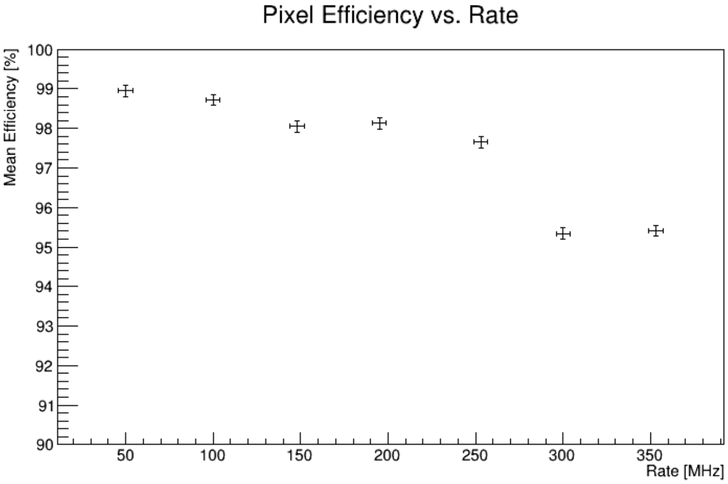

Figure 34: The mean efficiency as a function of the rate.

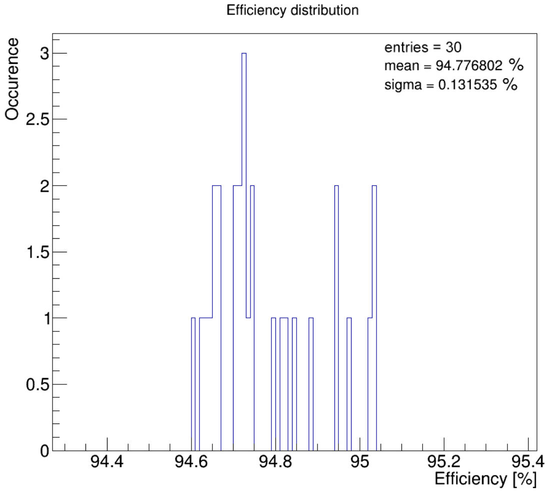

Figure 35: A distribution of 30 efficiency measurements. Each measurement was done for the rows 40-60.

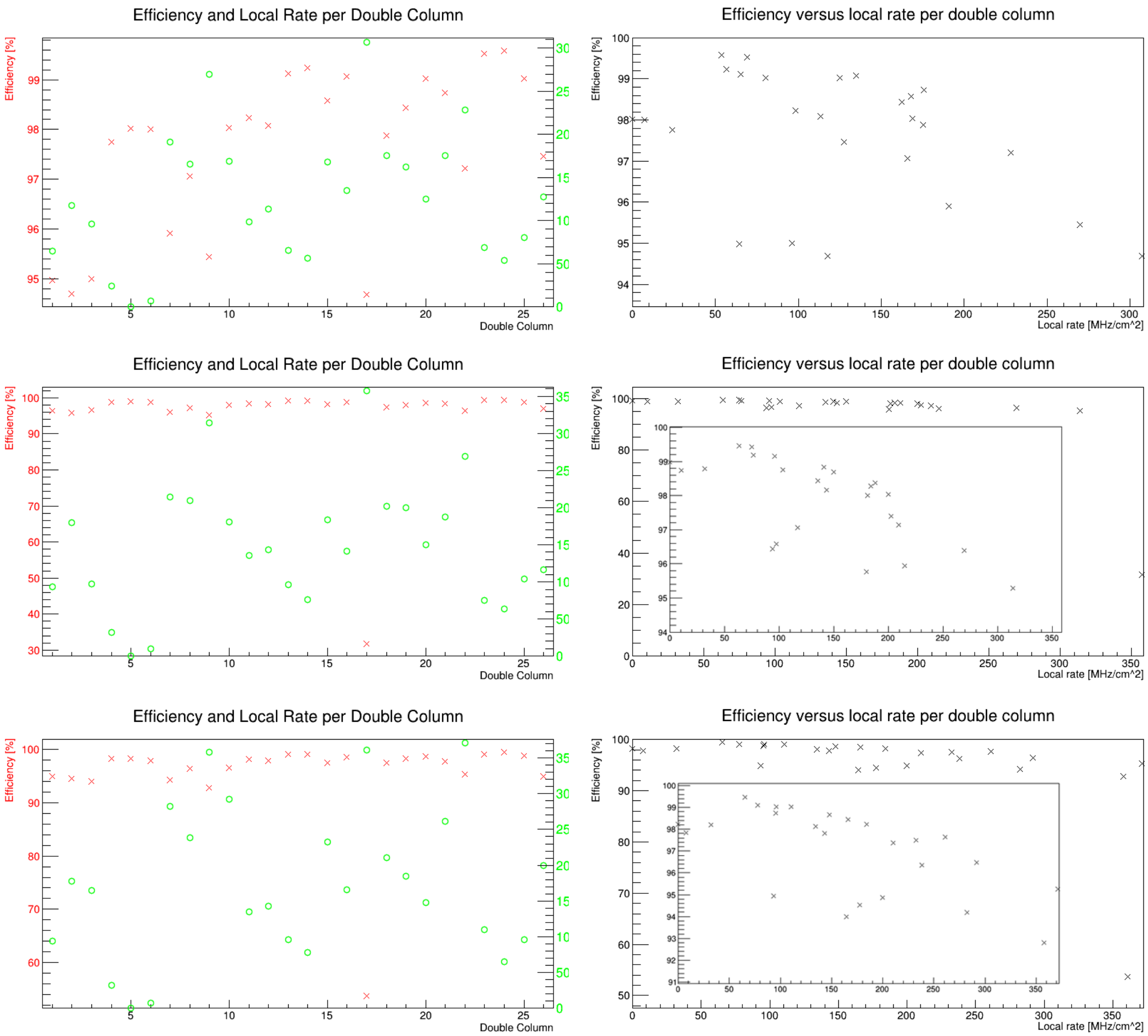
Efficiency and Local Rate per Double Column

Efficiency versus local rate per double column

Efficiency and Local Rate per Double Column

Efficiency versus local rate per double column

Efficiency and Local Rate per Double Column

Efficiency versus local rate per double column

Figure 36: Left: The efficiency (x) and the local rate (o) (cf. eq. 3) as a function of the double column.
Right: The efficiency as a function of the local rate.
The plots contain the data, starting on top, from the efficiency maps for 253 $\frac{MHz}{cm^2}$, 300 $\frac{MHz}{cm^2}$ and 353 $\frac{MHz}{cm^2}$.

5 Conclusion

The electrical high rate test produces, indeed, clusters of pixel hits at a tunable rate. Moreover, the rate agrees well with estimates which allow to predict the measured rate and program the data generator accordingly. However, high rates can only be measured with a specific choice of cables.

The accuracy of rate measurements depends on the amount of statistics, as expected. Yet, the required amount of statistics depends on the randomness of the readout.
Using a total of 100,000 triggers yielded an error of about 2 $\frac{MHz}{cm^2}$. The total amount of triggers was split using a **for loop**. In future experiments, a more sophisticated method to realise a random readout might help to decrease the necessary amount of triggers.

Synchronising the internal clocks of the data generator and the testboard proved to be important to control the amount of non-zero events and the amount of hits within each. With the clocks being synchronised, the pulse length does not matter when it comes to rate calculation, since the contributions of the edges and between are very reproducable and can be included in the estimate.
However, for most measurements the pulse length of one clock cycle is the easiest to handle as there are only hits in one clock cycle, per pulse.

Furthermore, the setup was successfully used to test the chip efficiency. The mean efficiency per pixel was found to be over 98 % for rates below 150 $\frac{MHz}{cm^2}$. Comparing the result shown in figure 34, with data obtained by X-ray experiments, the efficiency is already relatively low even below 150 $\frac{MHz}{cm^2}$. The reason for this difference is attributed to the different amount of hits per non-zero event. While in this experiment, there are about 80 hits in a non-zero event, there are only about 3 hits per non-zero event using X-rays at the same rate. Similar is the situation for the affected double columns. In this experiment, an affected double column contains usually about 5 hits, while there is rarely more than one hit per double column using an X-ray setup.
Therefore, in an affected double column the rate can easily reach 100 $\frac{MHz}{cm^2}$ or more.
To increase the comparability, the amount of wires per cable could be reduced to decrease the amount of hits caused by one pulse.

Looking at the rates in the double columns separately, the expected decrease of the efficiency with increasing rate is merely hinted. It is unclear why there is a fluctuation of the efficiency, even at relatively low rates, of up to roughly 4 %.

6 Possible Further Studies

An issue encountered with the actual setup, was the mechanical sensitivity of the excitation harness. Connecting and disconnecting cables can require a strength which is enough to pull a wire from the ROC. As all the wires are tightly compressed, when focusing them on the ROC, the wire will not return, once it has been pulled away.
This could be avoided by using e.g. a PCB as interconnection between the excitation harness and the data generator. The PCB could be part of a fixed structure, such that the user does hardly touch the excitation harness, once the ROC has been attached.

Generally, the control over the cluster position should be increased. At the same time, one could decrease the amount of wires per cable. Ideally, the wires should be connected separately, such that the distinction of cables and wires becomes redundant.
As a suggestion, one could place the wires on top of the Kapton foil in a well defined pattern. Since the patter is known, this would enable the determination of the cluster position.

7 Acknowledgments

I would like to thank Prof. Dr. Rainer Wallny for making this work possible, and letting me be part of the very enjoyable and helpful atmosphere. Furthermore, I would like to thank Dr. Andrey Starodumov and Dr. Wolfram Erdmann for their assistance and support during the project.

References

[1] The information used in the introduction was partially taken from the *CMS TECHNICAL DESIGN REPORT FOR THE PIXEL DETECTOR UPGRADE*,
ISBN 978-92-9083-380-2

[2] D.Kotlinski, R.Baur, K.Gabathuler, R.Horisberger, R.Schnyder and W.Erdmann, *Readout of the CMS Pixel Detector.*,
http://ph-collectif-lecc-workshops.web.cern.ch/ph-collectif-lecc-workshops/LEB00_Book/tracker/kotlinski.pdf (online 20.08.2012)

[3] The original picture was taken from a presentation of Jorgen Beck Hansen, “Physics at run 2”.

[4] The original pictures are taken from
User Manual, “DG2020A, P3410, & P3420”, *Data Generator and Pods*,
Sony/Tektronix Corporation, P.O. Box 5209, Tokyo Int’l, Tokyo 100-31 Japan,
Tektronix, Inc., P.O. Box 1000, Wilsonville, OR 97070-1000

8 Appendix

Figure 37, 38 and 39 show all pulse length scans (cf. section 4.4). Since the data generator did run with the clock of the testboard, the unit length of the pulse is given by 25 ns.

All efficiency maps and their analyses are summarised in figure 40, 41 and 42. The error in the rate is $\approx 2 \frac{MHz}{cm^2}$ according to figure 27.

All important programs and root makros which where used can be found on the provided CD ROM. A brief description is given in the following.

dceff1.C Takes an efficiency map (pa.py) as input and outputs the efficiency and local rate per double column as well as the efficiency as a function of the rate for each double column.

double.py performs the desynchronisation test as shown in figure 29. The function adc2() defines the sequence and is not given by default. It can, though, easily be rewritten using the adc() function, given in the file containing the testboard functions (DTB.py).

doubleC.py performs the desynchronisation test as shown in, e.g. figure 30. This test also makes use of the adc2() function.

eff.cxx takes an efficiency map as input provided by either pixelalive.py or pa.py. In the former case, it produces three pixel efficiency plots. One for all pixels, a second one for all affected double columns and a third for all clusters. In case of a map, provided by the pa.py program, it produces the efficiency for all pixels only, as for instance in figure 33.

efferror.C produces the plot shown in figure 35. The data is hardcoded.

effhisto1.C produces the plot shown in figure 34. The data is hardcoded.

functions.py provides a couple of functions to use the pulse height calibration data.

lhe.py produces 5 ROC maps containing single LHEs, as e.g. in figure 17.

map.py measures the rate and produces a ROC map, a hits per non-zero event distribution, a non-zero event per loop distribution and a pulse height distribution.

pa2.py performs an efficiency test and produces an efficiency map. It arms each pixel separately (instead of a whole row) and was used for debugging.

pa-error.py performs numerous efficiency tests. It provided the data for the efferror.C makro. In the beginning, a rate measurement is included to avoid a reinitialisation of the ROC.

pa.py performs an efficiency test and produces an efficiency map. It performs a rate measurement in the beginning, to avoid a reinitialisation of the ROC.

param.py contains the testing parameters used in map.py, pixelalive.py, pa.py, pa2.py, lhe.py and rate-vs-thr.py

pixelalive.py performs an efficiency test and produces an efficiency map.

rate-to-histo.py takes a text file containing the output of map.py and produces a rate distribution.

rate-vs-thr.py performs rate measurements while sweeping through an interval of $V_{thrComp}$. It produces a plot as show in figure 22.

scan-tct.py performs a pulse length scan as shown in figure 23. The synchronising signal must be added to the sequence.

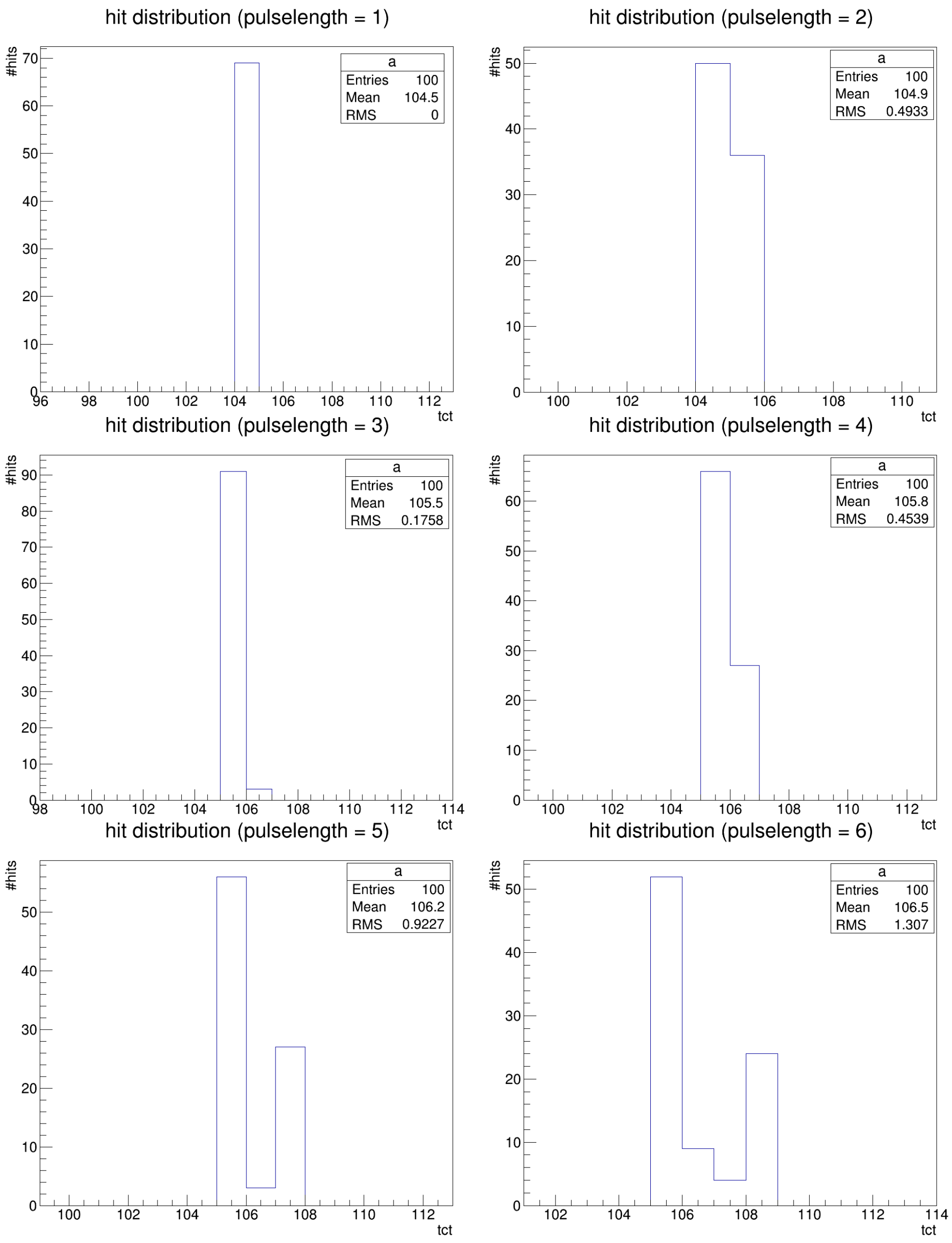
hit distribution (pulselength = 1)

hit distribution (pulselength = 2)

hit distribution (pulselength = 3)

hit distribution (pulselength = 4)

hit distribution (pulselength = 5)

hit distribution (pulselength = 6)

Figure 37: The amount of hits as a function of *tct*. The unit length of a pulse is 25 ns.

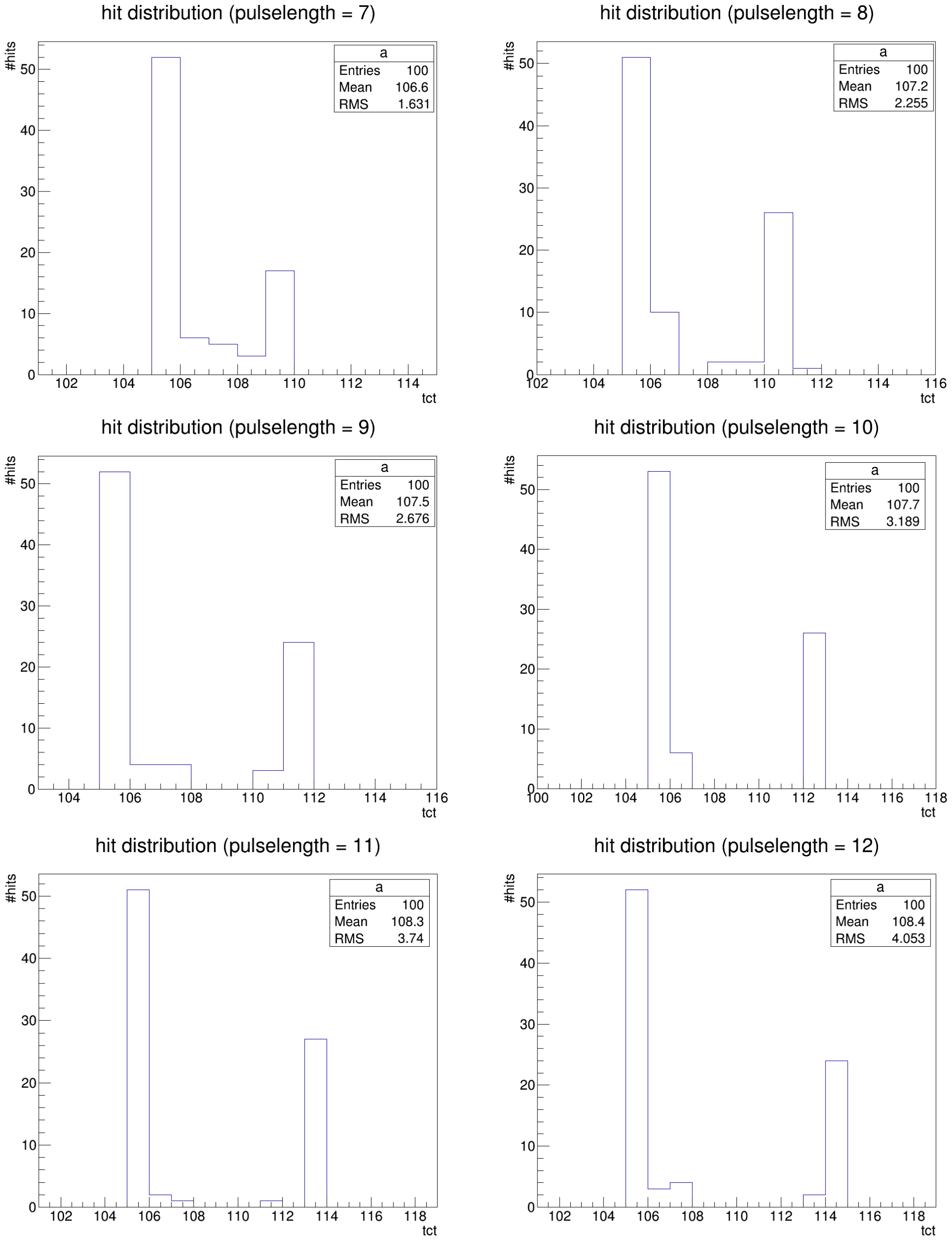

Figure 38: The amount of hits as a function of *tct*. The unit length of a pulse is 25 ns.

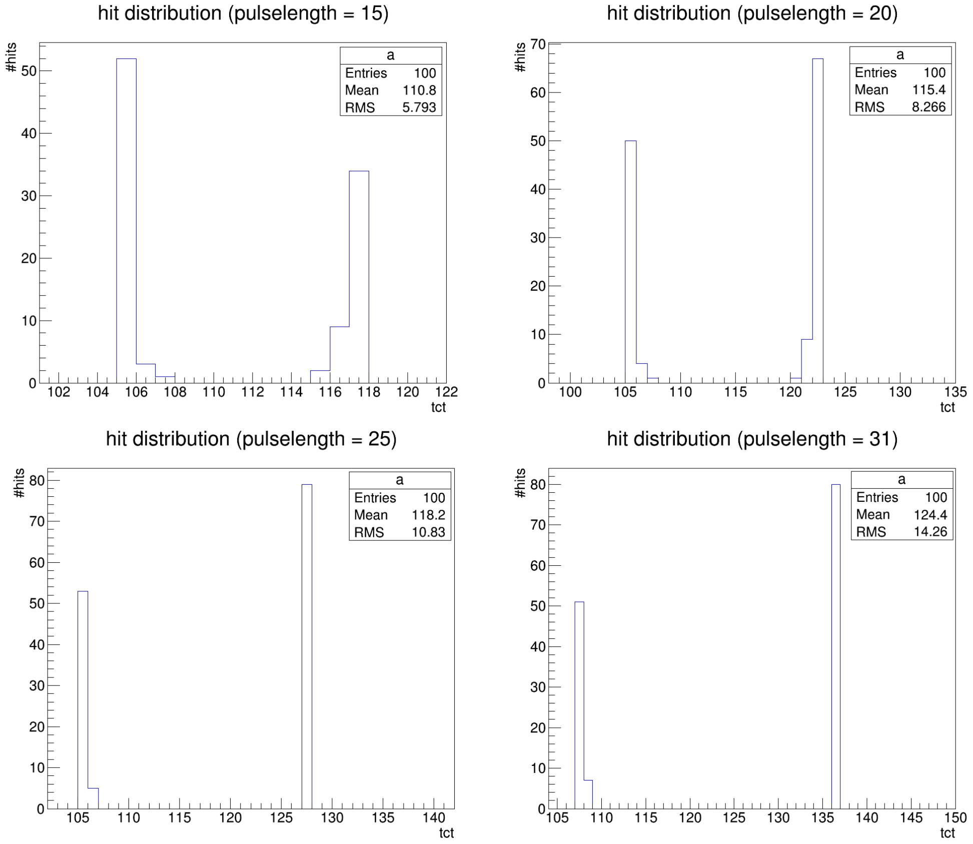

Figure 39: The amount of hits as a function of *tct*. The unit length of a pulse is 25 ns.

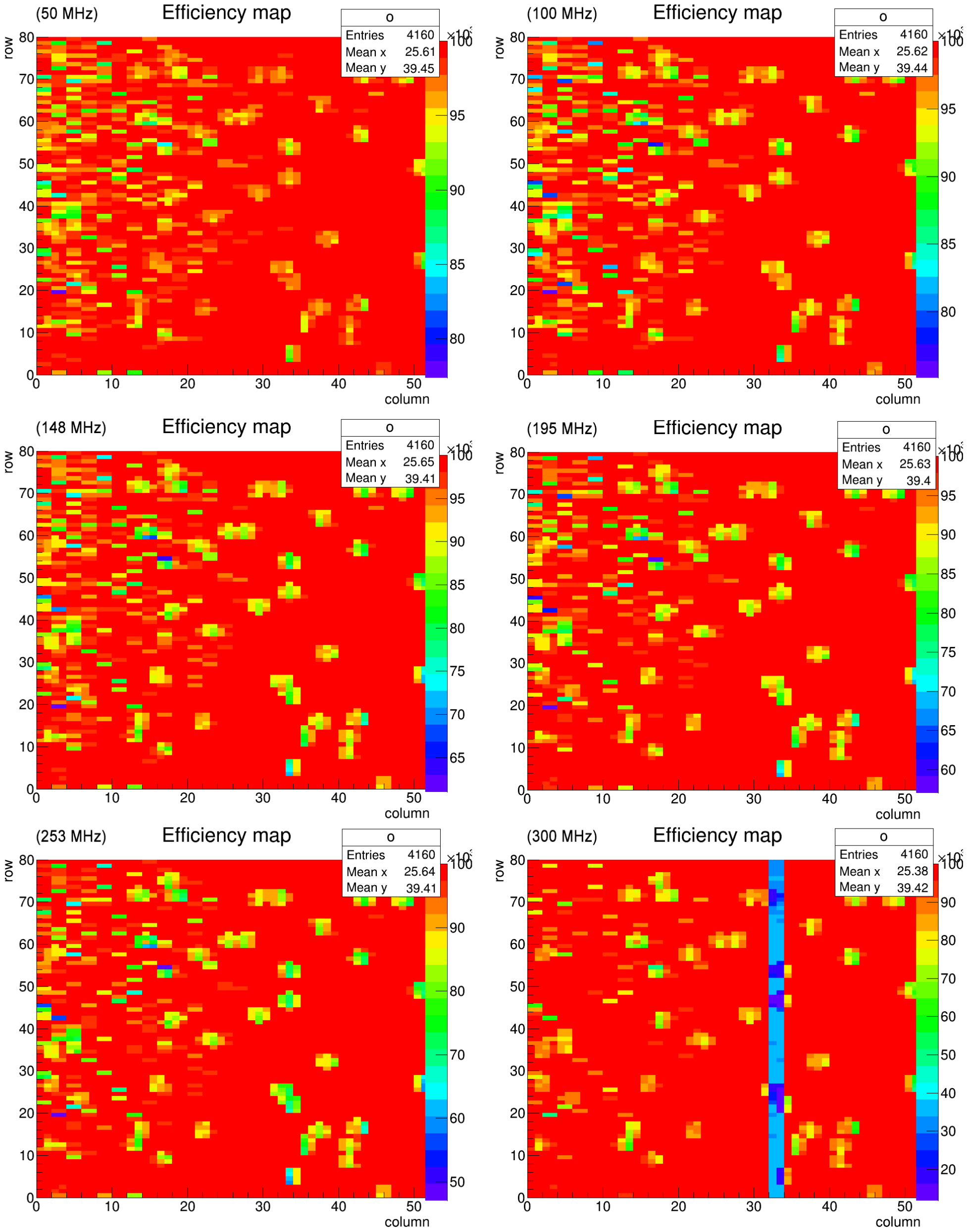

Figure 40: Efficiency maps, where the pixel efficiency is shown as a function of position. The rate is shown in the top left corner of each map.

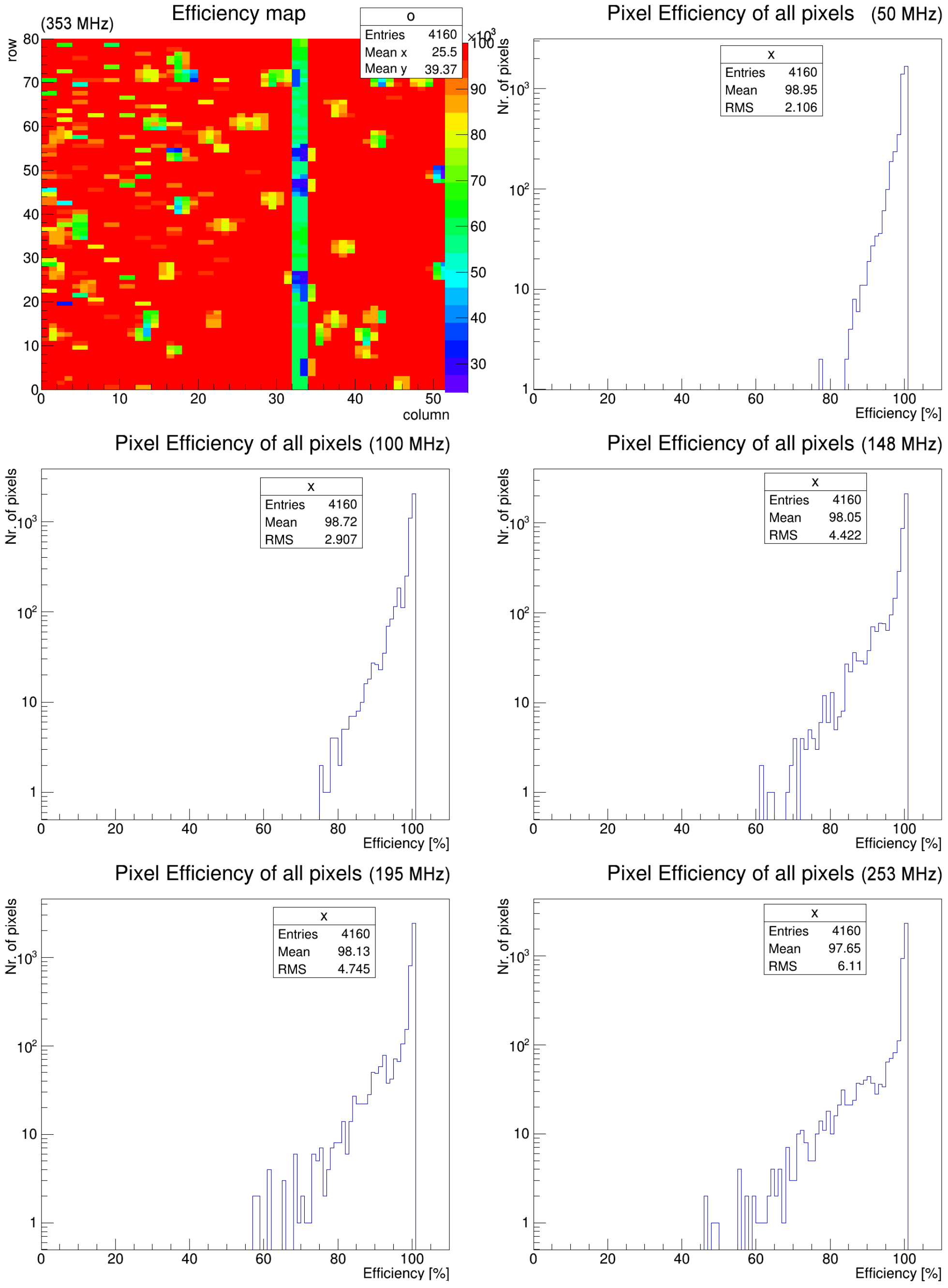

Figure 41: Efficiency map and plots, where the pixel efficiency is shown as a function of position and the amount of pixels is shown as a function of their efficiency, respectively. The rate is shown in the top right or top left corner of each plot or map, respectively.

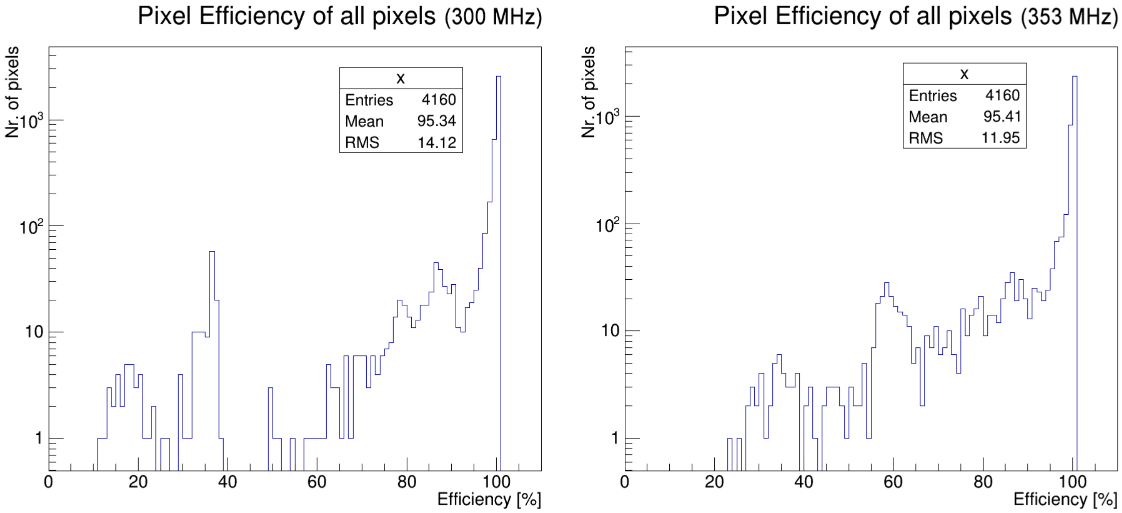

Figure 42: Pixel efficiency plots, where the amount of pixels is shown as a function of their efficiency. The rate is shown in the top right corner of each plot.

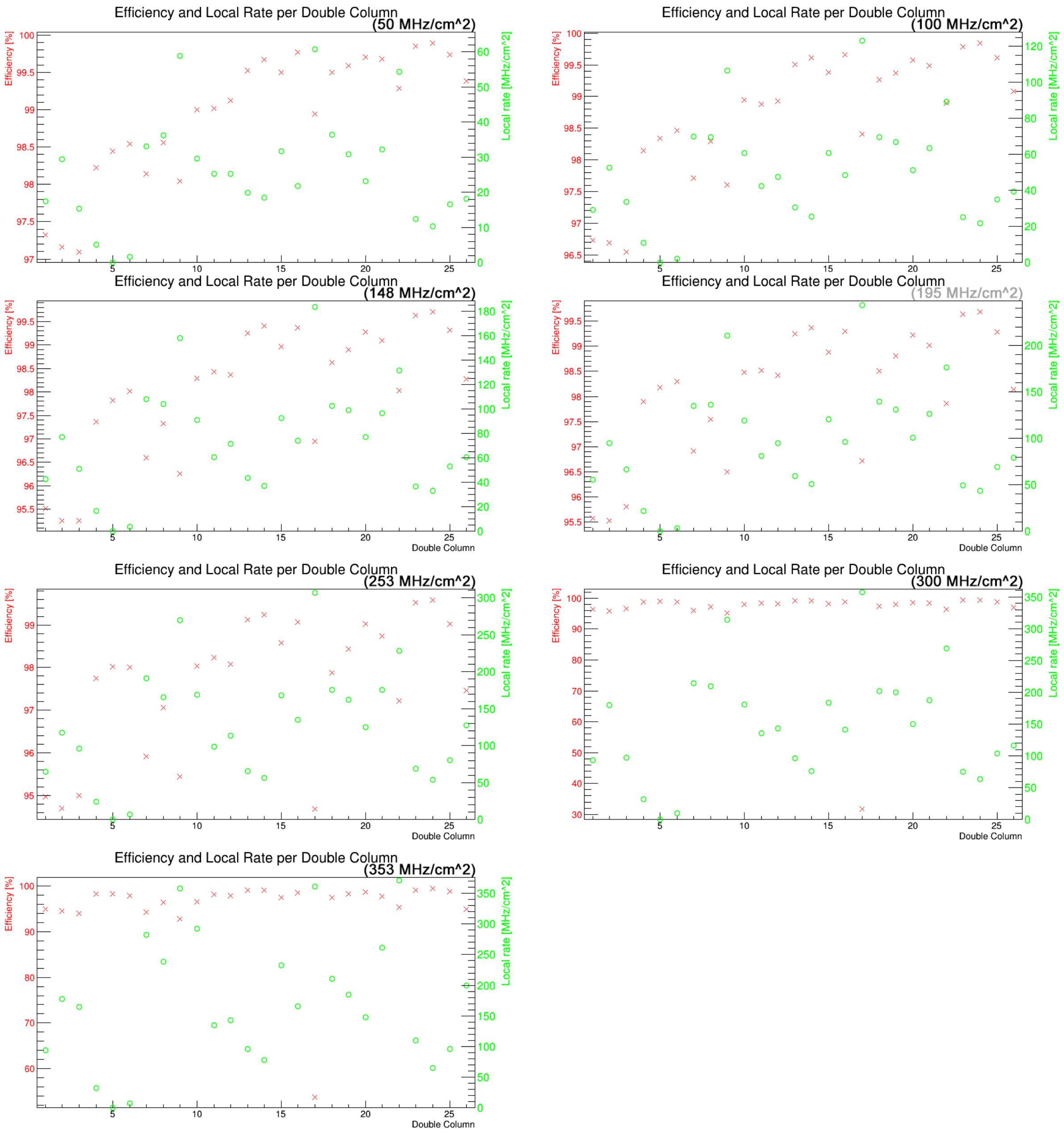

Figure 43: The efficiency (x) and the local rate (o) (cf. equation 3) as a function of the double column. The total rate is shown in the top right corner of each plot.

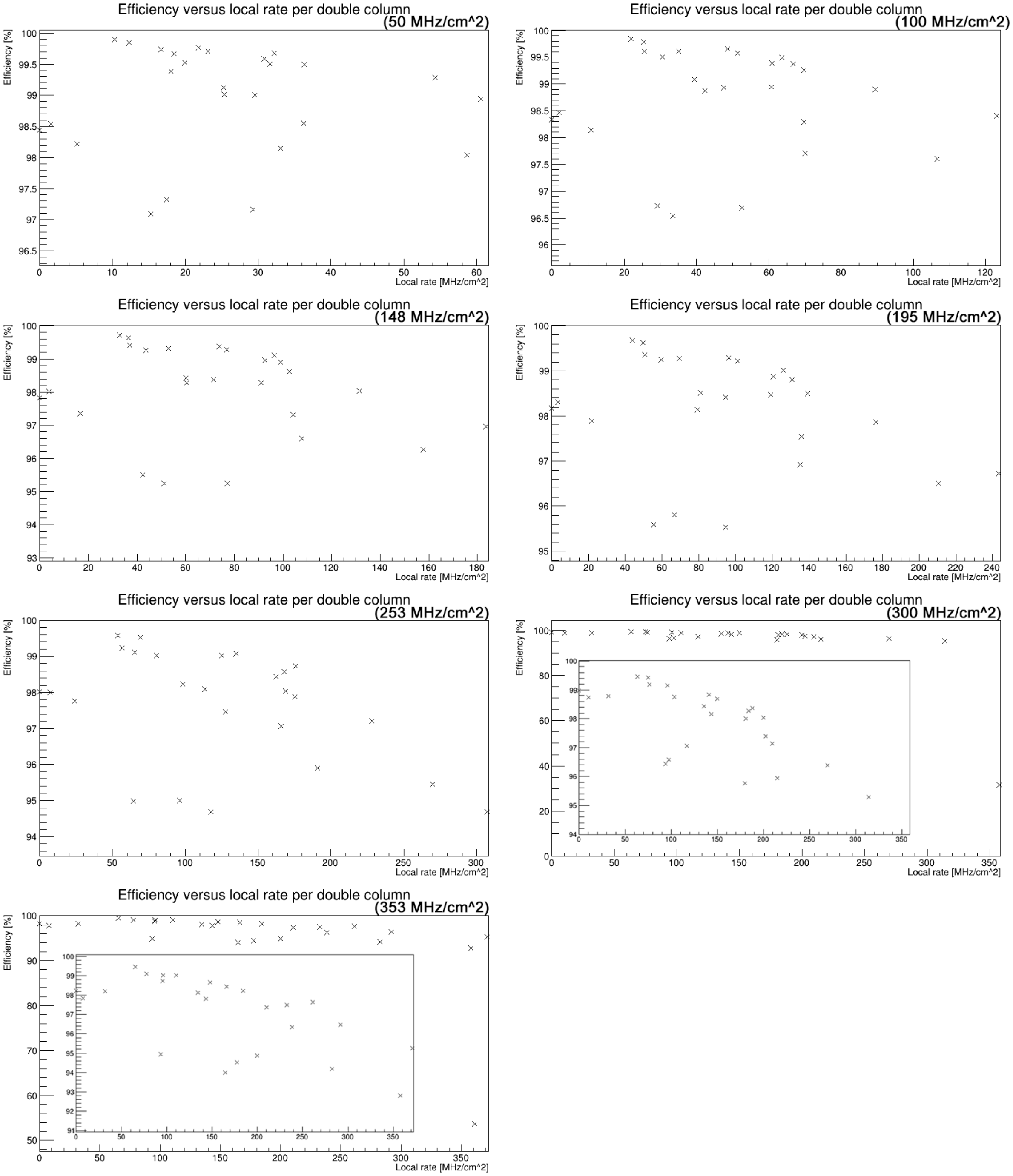

Figure 44: The efficiency as a function of the local rate (cf. equation 3) for each double column. The total rate is shown in the top right corner of each plot.